A DISSERTATION

FOR THE DEGREE OF DOCTOR OF PHILOSOPHY

Bone Regeneration by Mesenchymal Stem Cell Sheets Overexpressing BMP-7 in Canine Bone Defects

개의 결손골 모델에서 BMP-7 과발현 유도 중간엽 줄기세포 시트의 골재생 효과

by

Yongsun Kim

MAJOR IN VETERINARY SURGERY

DEPARTMENT OF VETERINARY MEDICINE

GRADUATE SCHOOL OF

SEOUL NATIONAL UNIVERSITY

August 2016

Bone Regeneration by Mesenchymal Stem Cell Sheets Overexpressing BMP-7 in Canine Bone Defects

by

Yongsun Kim

Supervised by

Professor Oh-Kyeong Kweon

A Dissertation submitted to
the Graduate School of Seoul National University
in partial fulfillment of the requirement
for the degree of Doctor of Philosophy in Veterinary Surgery

June 2016

MAJOR IN VETERINARY SURGERY
DEPARTMENT OF VETERINARY MEDICINE
GRADUATE SCHOOL OF
SEOUL NATIONAL UNIVERSITY

August 2016

Bone Regeneration by Mesenchymal Stem Cell Sheets Overexpressing BMP-7 in Canine Bone Defects

Advisor: Professor Oh-Kyeong Kweon

Submitting a doctoral thesis of veterinary surgery

May 2016

Major in Veterinary Surgery
Department of Veterinary Medicine
Graduate School of Seoul National University

Yongsun Kim

Confirming the doctoral thesis written by Yongsun Kim

June 2016

Chair Professor	Wan Hee Kim	_____
Vice Chair Professor	Oh-Kyeong Kweon	_____
Member Professor	Min Cheol Choi	_____
Member Professor	Heung-Myong Woo	_____
Member Professor	Byung-Jae Kang	_____

Bone Regeneration by Mesenchymal Stem Cell Sheets Overexpressing BMP-7 in Canine Bone Defects

Yongsun Kim

(Supervised by Professor Oh-Kyeong Kweon)

Major in Veterinary Surgery
Department of Veterinary Medicine
Graduate School of Seoul National University

ABSTRACT

Successful repair of bone defect injuries is a major issue in reconstructive surgery. The necessary elements for bone healing include osteogenic cells, osteoinductive growth factors, and osteoconductive matrix. Multipotent mesenchymal stem cells (MSCs) and MSC sheets have potential for bone regeneration. Bone morphogenetic protein 7 (BMP-7) has been shown to possess strong osteoinductive properties. In addition, composite polymer/ceramic scaffolds such as poly ε-caprolactone (PCL)/β-tricalcium phosphate (β-TCP) are widely used to repair large bone defects.

In the first chapter, the *in vitro* osteogenic potential of canine adipose-derived MSCs (Ad-MSCs) and Ad-MSC sheets are compared. Composite PCL/β-TCP scaffolds seeded with Ad-MSCs or wrapped with osteogenic Ad-MSC sheets (OCS) were also fabricated and their *in vivo* osteogenic potential was assessed after transplantation into critical-sized bone defects in dogs. The alkaline phosphatase (ALP) activity in osteogenic Ad-MSCs (O-MSCs) and OCS was significantly higher than that of undifferentiated Ad-MSCs (U-MSCs). *ALP, runt related transcription factor 2 (RUNX2), osteopontin,* and *BMP-7* mRNA levels were up-regulated in O-MSCs and OCS compared to those in U-MSCs. The amount of newly formed bone was greater in PCL/β-TCP/OCS and PCL/β-TCP/O-MSCs/OCS than in the PCL/β-TCP/U-MSCs and PCL/β-TCP/O-MSCs groups. Although there was no difference between *in vitro* osteogenic genes expression of O-MSCs and OCS, the new bone formation was greater in the scaffold wrapped with OCS than the scaffold seeded U-MSCs and O-MSCs. Consequently, it was suggested that OCS could be used as an osteogenic matrix in canine critical-sized bone defects.

OCS is difficult to handle and culture for more than two weeks; however, undifferentiated Ad-MSC sheets (UCS) are easy to culture and handle. The osteogenic capacity of USCs could be enhanced by canine BMP-7 gene transduction using a lentiviral system. Demineralized bone matrix (DBM), as defect filling and osteoinductive materials in large bone defects, was combined in a subsequent study. Combination of UCS overexpressing BMP-7

and DBM is supposed to be potential vehicles for bone healing.

In the second chapter, canine Ad-MSCs overexpressing BMP-7 (BMP-7-MSCs) were produced and sheets formed from these cells (BMP-7-CS) were compared with Ad-MSC sheets for *in vitro* osteogenic potential. BMP-7-CS with and without DBM, were transplanted into critical-sized bone defects *in vivo* and osteogenesis was assessed. BMP-7 mRNA and protein levels were up-regulated in BMP-7-MSCs compared to those in Ad-MSCs. The ALP activity in Ad-MSC sheets and BMP-7-CS were significantly higher than that in Ad-MSCs. *ALP, RUNX2, osteopontin, BMP-7, transforming growth factor-β* and *platelet-derived growth factor-β* mRNA levels were up-regulated in BMP-7-CS compared to levels in Ad-MSCs and Ad-MSC cell sheets. BMP-7-CS showed the highest osteogenic abilities *in vitro*. The amount of newly formed bone and neovascularization were greater in BMP-7-CS and BMP-7-CS/DBM groups than in control groups. However, the BMP-7-CS/DBM group had more mineralized particles inside the defect sites than the BMP-7-CS group. As a result, it was suggested that a combination of BMP-7-CS and DBM could be used as osteogenic materials in canine critical-sized bone defects.

BMP-7-CS not only provides BMP-7 producing MSCs but also produce osteogenic and vascular trophic factors. The combination of these cells with the osteoinduction and osteoconduction properties of DBM could result in synergy during bone regeneration. Thus, transplantation of BMP-7-CS and

DBM could be used as an alternative treatment modality in bone tissue engineering.

Keywords: mesenchymal stem cell sheets, BMP-7, DBM, osteogenesis, bone defects, dogs

Student number: 2009-21616

CONTENTS

CHAPTER II

Osteogenic Potential of Adipose-Derived Mesenchymal Stem Cell Sheets Overexpressing Bone Morphogenetic Protein-7 in Canine Bone Defects

LIST OF ABBREVIATIONS

3-D	Three-dimensional
A2-P	L-ascorbic acid 2-phosphate
Ad-MSCs	Adipose-derived mesenchymal stem cells
ALP	Alkaline phosphatase
ARS	Alizarin red s
AXIN2	Axis inhibition protein 2
BMP	Bone morphogenetic protein
BMP-7-CS	Adipose-derived mesenchymal stem cell sheets overexpressing bone morphogenetic protein-7
BMP-7-MSCs	Adipose-derived mesenchymal stem cells overexpressing bone morphogenetic protein-7
cPPT	Central polyprine tract
CT	Computed Tomography
DBM	Demineralized bone matrix
DPBS	Dulbecco's phosphate-buffered saline
ECM	Extracellular matrix
GAPDH	Glyceraldehyde 3-phosphate dehydrogenase
GFP	Green fluorescent protein
H&E	Hematoxylin and eosin
HA	Hydroxyapatite
LRT	Long terminal repeat
MSCs	Mesenchymal stem cells
O-MSCs	Osteogenic adipose-derived mesenchymal stem cells

OCS	Osteogenic adipose-derived mesenchymal stem cell sheets
PCL	Poly ε-caprolactone
PDGF-β	Platelet-derived growth factor-β
pNPP	p-nitrophenyl phosphate
qRT-PCR	Quantitative reverse transcription polymerase chain reaction
RRE	Rev-responsible element
RSV	Rous sarcoma virus U3
RUNX2	Runt related transcription factor 2
SDS	Sodium dodecyl sulfate
TGF-β	Transforming growth factor-β
U-MSCs	Undifferentiated adipose-derived mesenchymal stem cells
UCS	Undifferentiated adipose-derived mesenchymal stem cell sheets
VEGF	Vascular endothelial growth factor
WPRE	Woodchuck hepatitis virus post-transcriptional regulatory element
β-TCP	β-tricalcium phosphate

LIST OF FIGURES

LIST OF TABLES

GENERAL INTRODUCTION

The reconstruction of large bone defects resulting from trauma, tumor resection, infection, and skeletal abnormalities remains an important clinical problem. For the treatment of bone defects, it is necessary to consider the following fundamental concepts: 1) synthesis of bone through osteogenesis by osteogenic cells, 2) osteoinduction resulting in the recruitment of mesenchymal cells and differentiation into osteogenic cells, and 3) osteoconduction that acts as a scaffold for new bone ingrowth (Calori and Giannoudis, 2011). Bone graft materials possess these properties, and thus bone grafting is performed to augment bone regeneration. Autologous bone grafting is considered the most appropriate technique to treat bone defects, because it combines all properties required in a bone graft materials. However, this method has several drawbacks, including donor site morbidity, chronic pain, and inadequate volume of graft material (Cancedda *et al*., 2007).

To provide an alternative for autologous bone grafting and to accelerate bone regeneration, various strategies have been studied. Cell-based tissue engineering is a promising alternative approach to bone regeneration. In particular, mesenchymal stem cells (MSCs) show great potential for therapeutic use in bone tissue engineering due to their capacity for osteogenic differentiation and regeneration (Kang *et al.,* 2012). However, transplanted

single-cell suspensions do not attach, survive, or proliferate in target tissues (Yamato and Okano, 2004). Cell sheets are beneficial for cell transplantation because cell-cell junctions and endogenous extracellular matrix (ECM) are preserved. This ensures homeostasis in the cellular microenvironment for the sustained long-term delivery of growth factors and cytokines that promote tissue repair.

Osteoblast differentiation of multipotent stem cells is known to be regulated by bone morphogenetic proteins (BMPs), which are members of the transforming growth factor (TGF) superfamily, and many studies have demonstrated that BMPs stimulate bone formation (Alaee *et al*., 2014; Cook *et al*., 1994; Wang *et al*., 1990). The development of gene-modified tissue engineering has provided an attractive approach with great potential for repairing bone defects. Lentiviral based BMP-7 gene therapy systems offering prolonged gene expression might be ideal for the treatment of large bone defects that require a long-term osteoinductive stimulus, or in cases where the host biological environment has been compromised (Hsu *et al*., 2007; Sugiyama *et al*., 2005).

Three-dimensional structural scaffolds have also been developed to replace autologous bone grafts. Synthetic bone substitutes such as collagen, hydroxyapatite (HA), β-tricalcium phosphate (β-TCP), and synthetic polymers are currently available for bone tissue regeneration. Ceramic scaffolds that consists of HA and β-TCP have been widely used to repair bone defects in

clinical applications as since they have good biocompatibility and a microstructure similar to that of the mineral component of natural bone (Guan *et al*., 2015; Kondo *et al*., 2005). Poly ε-caprolactone (PCL), a polymer-based composite, has also been used for bone tissue engineering based on its biodegradability and biocompatibility, as well as its minimal induction of an inflammatory response (Ali *et al*., 1993; Wei and Ma 2004). Among bone substitutes, demineralized bone matrix (DBM) has been effective and widely used clinically. DBM expose BMP and other peptide-signaling molecules on the retained collagen skeleton to improve osteoinductive and osteoconductive potential (Mauney *et al*., 2005). Growth factors such as insulin-like growth factor-1 and TGF-β have also been identified in DBM (Wildemann *et al*., 2007).

This study was performed to investigate strategies for enhancing bone regeneration by transplantation of Ad-MSC sheets into critical-sized bone defects in dogs. First, composite PCL/β-TCP scaffolds seeded with Ad-MSCs or wrapped with osteogenic cell sheets were transplanted into bone defects and the osteogenic effects were evaluated (Chapter I). Second, Ad-MSCs overexpressing BMP-7 were produced and sheets were formed from these cells. Ad-MSC sheets overexpressing BMP-7 with DBM particles were assessed for their osteogenic potential after transplantation into the bone defects (Chapter II).

CHAPTER I

Comparison of Osteogenesis between Adipose-derived Mesenchymal Stem Cells and Their Sheets on Poly ε-Caprolactone/β-Tricalcium Phosphate Composite Scaffolds in Canine Bone Defects

ABSTRACT

Composite polymer/ceramic scaffolds such as poly ε-caprolactone (PCL)/β-tricalcium phosphate (β-TCP) are widely used to repair large bone defects, while mesenchymal stem cell (MSC) sheets are used to enhance their regenerative capacity. The present study investigated the in vitro osteogenic potential of canine adipose-derived MSCs (Ad-MSCs) and Ad-MSC sheets. Composite PCL/β-TCP scaffolds seeded with Ad-MSCs or wrapped with osteogenic Ad-MSC sheets (OCS) were also fabricated and their osteogenic potential was assessed following transplantation into critical-sized bone defects in dogs. The alkaline phosphatase (ALP) activity of osteogenic Ad-MSCs (O-MSCs) and OCS was significantly higher than that of undifferentiated Ad-MSCs (U-MSCs). The *ALP, runt related transcription*

factor 2, osteopontin, and *bone morphogenetic protein 7* mRNA levels were upregulated in O-MSCs and OCS as compared to U-MSCs. In a segmental bone defect model, the amount of newly formed bone was greater in PCL/β-TCP/OCS and PCL/β-TCP/O-MSCs/OCS than in the other groups. Hence, OCS exhibit strong osteogenic capacity, and OCS combined with a PCL/β-TCP composite scaffold stimulated new bone formation in a canine critical-sized bone defect. These results suggest that the PCL/β-TCP/OCS composite has potential for clinical applications in bone regeneration and could be used as an alternative treatment modality in bone tissue engineering.

INTRODUCTION

Synthetic bone substitutes such as collagen, hydroxyapatite (HA), β-tricalcium phosphate (β-TCP), and synthetic polymers are currently available for bone tissue regeneration. Ceramic scaffolds that consists of HA and β-TCP have been widely used to repair bone defects in clinical applications, since they have good biocompatibility and a microstructure similar to the mineral component of natural bone (Guan *et al.,* 2015; Kondo *et al.,* 2005). Poly ε-caprolactone (PCL), a type of polymer-based composite, has also been used for bone tissue engineering owing to its biodegradability, biocompatibility, and low inflammatory response (Ali *et al.,* 1993; Wei and Ma 2004). Some recent studies have examined the feasibility of using composite polymer/ceramic scaffolds such as PCL/β-TCP so as to combine the advantages of each material (Fujihara *et al.,* 2005; Simpson *et al.,* 2008; Wei and Ma 2004).

Cell-based tissue engineering is a promising alternative approach to bone regeneration. In particular, mesenchymal stem cells (MSCs) show great potential for therapeutic use in bone tissue engineering due to their capacity for osteogenic differentiation and regeneration (Kang *et al.,* 2012). However, transplanted single-cell suspensions do not attach, survive, or proliferate on target tissues (Yamato and Okano, 2004). To overcome this limitation, cell sheet technology has been developed to enhance the regenerative capacity of

tissue-engineered products (Akahane *et al.*, 2008; Long *et al.*, 2014). Cell sheets are beneficial for cell transplantation because they preserve cell-cell junctions as well as endogenous extracellular matrix (ECM), thereby ensuring homeostasis of the cellular microenvironment for the delivery of growth factors and cytokines that promote the tissue repair over a prolonged period of time.

I hypothesized that a combination construct of synthetic scaffolds with MSCs or MSC sheets could accelerate and enhance bone regeneration in large bone defects. In this study, canine adipose-derived (Ad-)MSC sheets were generated by cell sheet technology, and the osteogenic potential of Ad-MSCs and Ad-MSC sheets was investigated *in vitro*. In addition, composite PCL/β-TCP scaffolds seeded with Ad-MSCs or wrapped with osteogenic cell sheets were constructed and assessed for their osteogenic potential after transplantation into critical-sized bone defects in dogs.

MATERIALS AND METHODS

1. Isolation and Culture of Canine Ad-MSCs

The study protocol was approved by the Institutional Animal Care and Use Committee of Seoul National University (SNU-140801-1). MSCs derived from canine hip adipose tissue were isolated and characterized (Ryu *et al.*, 2009). The tissue was collected aseptically from the subcutaneous fat of a 2-year-old beagle dog under anesthesia, and washed with Dulbecco's phosphate-buffered saline (DPBS; Thermo Fisher Scientific Inc., USA), minced, then digested with collagenase type I (1 mg/ml; Sigma-Aldrich, St. Louis, USA) at 37℃ for 30–60 minutes with intermittent shaking. The suspension was filtered through a 100-μm nylon mesh and centrifuged to separate floating adipocytes from stromal cells. Pre-adipocytes in the stromal vascular fraction were plated at 8,000–10,000 cells/cm^2 in T175 culture flasks containing Dulbecco's modified Eagle's medium (Thermo Fisher Scientific Inc.) supplemented with 3.7 g/l sodium bicarbonate, 1% penicillin/streptomycin, 1.7 mM L-glutamine, and 10% fetal bovine serum (Thermo Fisher Scientific Inc.). Cells were incubated in a humidified atmosphere at 37℃ and 5% CO_2. Unattached cells and residual non-adherent red blood cells were removed after 24 hours by washing with PBS, and the culture medium was replaced every 2

days. Cells were used for experiments after the third passage.

2. Preparation of Osteogenic Cell Sheet (OCS) and Ad-MSCs Cultures

OCS were prepared as previously described (Akahane *et al.*, 2008). Briefly, Ad-MSCs were seeded at a density of 1×10^4 cells/cm^2 in a 100-mm culture dish and cultured in growth medium containing 0.1 μM dexamethasone (Sigma-Aldrich) and 82 μg/ml L-ascorbic acid 2-phosphate (A2-P, Sigma-Aldrich) for 10 days. As a positive control for Ad-MSCs induced to undergo osteogenic differentiation (O-MSCs), cells were seeded at the same density and cultured in growth medium containing 0.1 μM dexamethasone, 15 μg/ml A2-P, and 10 mM β-glycerophosphate (Sigma-Aldrich). Undifferentiated Ad-MSCs (U-MSCs; negative control) were cultured in unsupplemented growth medium for 10 days. Morphological changes in cells during culture were monitored under an inverted light microscope (Olympus Corp., Japan).

3. Alkaline Phosphatase (ALP) Activity Measurement

Cells cultured in 100-mm dishes were used for measurement of ALP activity using an ALP assay kit (Takara Bio Inc., Japan) according to the manufacturer's instructions. Briefly, p-nitrophenyl phosphate (pNPP) solution was prepared by dissolving 24 mg pNPP substrate in 5 ml ALP buffer. Cells were scraped into 200 μl extraction solution, homogenized, and sonicated. The cleared supernatant was collected after centrifugation at 13,000 × g and 4℃ for 10 minutes. A 50-μl volume of cell lysate supernatant was mixed with 50 μl pNPP substrate solution and incubated at 37°C for 30 minutes. After adding 50 μl stop solution (0.5N NaOH), absorbance was measured at 405 nm with a spectrophotometer.

4. Quantification of Mineralization

Alizarin Red S (ARS) staining was used to detect calcium mineralization. Cells cultured in 100-mm dishes for 10 days were washed twice with DPBS and fixed with 4% paraformaldehyde (Wako, Japan) at room temperature for 10 minutes. Cells were then washed three times with distilled water, and 3 ml of 40 mM ARS (Sigma-Aldrich; pH 4.1–4.3) were added to each dish, followed by incubation at room temperature for 20 minutes with gentle

shaking. Excess dye was removed by aspiration and cells were washed three times with distilled water. For quantification of staining, the ARS was solubilized in 2 ml of 10% cetylpyridinium chloride (Sigma-Aldrich) for 1 hour (Gregory *et al.*, 2004), and the absorbance at 570 nm was measured with a spectrophotometer.

5. Gene Expression Analysis

Total RNA was isolated from cells using the Hybrid-RTM RNA extraction kit (GeneAll Bio, Korea) according to the manufacturer's protocol. RNA concentration was determined by measuring optical density at 260 nm with a NanoDrop ND-1000 spectrophotometer (NanoDrop Technologies, USA). cDNA was synthesized from RNA using a commercially available cDNA synthesis kit (Takara Bio Inc.). Quantitative reverse transcription polymerase chain reaction (qRT-PCR) was carried out on an ABI 7300 Real-time-PCR system (Applied Biosystems, USA) and SYBR Premix Ex Taq (Takara Bio Inc.). Primer sequences are listed in Table 1.1. Expression levels of target genes were normalized to the level of glyceraldehyde 3-phosphate dehydrogenase (GAPDH), and quantitated with the ΔΔCt method (Livak and Schmittgen, 2001).

Table 1.1. Primers sequences used for quantitative reverse transcription PCR

Target gene		**Primer sequence (5'-3')**
RUNX2	Forward	TGTCATGGCGGGTAACGAT
	Reverse	TCCGGCCCACAAATCTCA
ALP	Forward	TCCGAGATGGTGGAAATAGC
	Reverse	GGGCCAGACCAAAGATAGAG
Osteopontin	Forward	GATGATGGAGACGATGTGGATA
	Reverse	TGGAATGTCAGTGGGAAAATC
Osteocalcin	Forward	CTGGTCCAGCAGATGCAAAG
	Reverse	GGTCAGCCAGCTCGTCACAGTT
BMP-7	Forward	TCGTGGAGCATGACAAAGAG
	Reverse	GCTCCCGAATGTAGTCCTTG
TGF-β	Forward	CTCAGTGCCCACTGTTCCTG
	Reverse	TCCGTGGAGCTGAAGCAGTA
AXIN	Forward	ACGGATTCAGGCAGATGAAC
	Reverse	CTCAGTCTGTGCCTGGTCAA
β-catenin	Forward	TACTGAGCCTGCCATCTGTG
	Reverse	ACGCAGAGGTGCATGATTTG
VEGF	Forward	CTATGGCAGGAGGAGAGCAC
	Reverse	GCTGCAGGAAACTCATCTCC
GAPDH	Forward	CATTGCCCTCAATGACCACT
	Reverse	TCCTTGGAGGCCATGTAGAC

6. Fabrication of PCL/β-TCP Scaffolds

PCL was dissolved in chloroform at 40℃. NaCl and β-TCP were ground and sieved, and granules between 25 and 33 μm were selected. β-TCP was prepared by calcination of nano-TCP (Merck, USA) at 1,000℃ for 4 hours. Selected NaCl granules were mixed with predetermined amounts of ceramic particles (1:1 = NaCl:PCL, 1.5:1 = ceramic:PCL, weight ratios). Combined powders were mixed with the PCL suspension to produce a homogeneous paste. Sheet-type porous scaffolds (50 × 25 mm, five layers) were constructed by extruding the gel paste onto a substrate using a three-dimensional (3-D) printing system (Figure 1.1). The shapes and sizes of the PCL/β-TCP scaffold were designed using a computer system. NaCl was removed by immersing the scaffold in deionized water to produce macro-sized pores in strut and the water replaced every 2 hours with fresh water at 30℃ after sufficient drying of the scaffold.

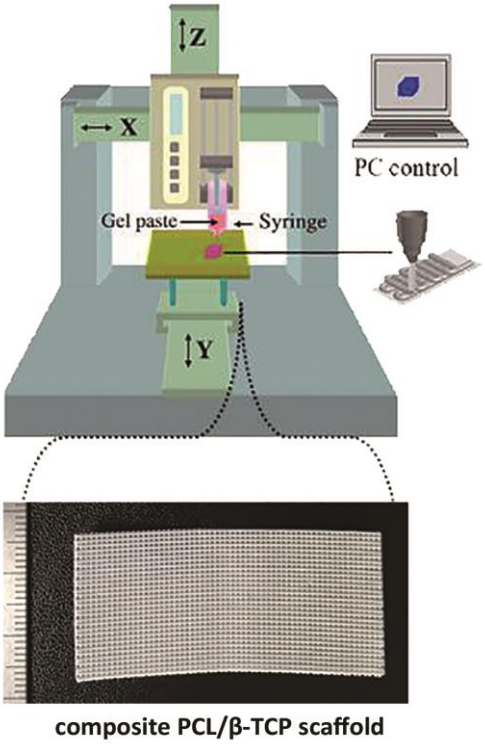

Figure 1.1. Photograph of a fabricated composite PCL/β-TCP scaffold. Sheet-type porous scaffolds (50 × 25 mm, five layers) were constructed by extruding the gel paste onto a substrate using a three-dimensional printing system.

7. Preparation of Scaffold with Ad-MSCs and Cell Sheet

Scaffolds were immersed in DPBS for 24 hours. Ad-MSCs (~ 1×10^6) were seeded on the scaffolds in a 100-mm dish for the PCL/β-TCP/U-MSCs group. After 24 hours of incubation, the medium was replaced with osteoinductive medium for the PCL/β-TCP/O-MSCs group. The culture was maintained for 10 days at 37℃ and 5% CO_2, and the medium was changed every 48 hours. For the PCL/β-TCP/OCS group, the scaffold was wrapped with four OCS after 10 days of culture. Cell-free scaffolds cultured in growth medium under the same conditions were used as controls.

8. Animal Experiments

Beagle dogs (n = 20; 2–3 years old) weighing 8.7 ± 1.4 kg were used in the study. Dogs were handled in accordance with the animal care guidelines of the Institute of Laboratory Animal Resources, Seoul National University, Korea. The dogs were assigned to one of five groups (n = 4 in each): PCL/β-TCP (control), PCL/β-TCP/U-MSCs, PCL/β-TCP/O-MSCs, PCL/β-TCP/OCS, and PCL/β-TCP/O-MSCs/OCS. The Institutional Animal Care and Use Committee of Seoul National University approved the experimental design. Dogs were medicated and anesthetized with tramadol (4 mg/kg by intravenous

(i.v.) injection; Toranzin; Samsung Pharmaceutical Co., Korea), propofol (6 mg/kg i.v.; Provive; Claris Lifesciences, Indonesia), and atropine sulfate (0.05 mg/kg by subcutaneous injection; Jeil Pharmaceutical Co., Korea). Anesthesia was maintained with isoflurane (Forane solution; Choongwae Pharmaceutical Co., Korea) at 1.5 minimum alveolar concentration throughout the procedure. Electrocardiography, pulse oximetry, respiratory gas analysis, and rectal temperature measurement were carried out using an anesthetic monitoring system (Datex-Ohmeda S/5; GE Healthcare, UK). Under sterile conditions, a craniomedial incision was made to the skin to expose the diaphysis of the left radius. A 15 mm-long segmental defect was made to the middle portion of the diaphysis using an oscillating saw (Stryker, USA). Overlying periosteum was also resected from the defect area. Defects were surrounded by the experimental scaffold. A nine-hole, 2.7-mm dynamic compression plate (DePuy Synthes, Switzerland) was placed on the cranial aspect of the radius. The soft tissue was closed with 3-0 polydioxanone sutures (Ethicon, USA), and the skin was closed with 4-0 nylon sutures. All the animals were bandaged for 2 days after operation. Operated limbs were weight-beared after removing bandage.

9. Micro-Computed Tomography (CT) for Bone Imaging

Dogs were sacrificed 12 weeks after implantation. The radius segment was excised, trimmed, and fixed in 10% formalehyde. Samples were scanned using a micro-CT system (Skyscan; Bruker Corp., Belgium) and 3-D images were reconstructed; the volume of newly formed bone within bone defects was calculated using the auxiliary software (Bruker Corp.).

10. Histological Analysis

After micro-CT measurement, specimens were decalcified in 8% nitric acid for 4 weeks at room temperature, then dehydrated through a graded series of alcohol, embedded in paraffin, sectioned at a thickness of 5 or 8 μm, and stained with hematoxylin and eosin (H&E) or Masson's trichrome according to standard protocols.

11. Statistical Analysis

Results are expressed as mean ± standard deviation. Statistical analysis was performed using SPSS v.21.0 software (IBM Corp., USA). Group means were

compared with the Kruskal-Wallis tests followed by Mann-Whitney U tests. A *p* value of less than 0.05 was considered statistically significant.

RESULTS

1. Cell Sheet Formation and Osteogenic Differentiation

U-MSCs and O-MSCs cultured for 10 days exhibited a spindle-shaped, fibroblast-like morphology with clearly delineated cell margins. However, OCS appeared to overlap and was stacked on top of one another, with indistinguishable cell-cell boundaries (Figure 1.2.A). The OCS was composed of two to four layers of cells surrounded by ECM (Figure 1.2.B), and it was easily detached by cell scraper (Figure 1.2.C). ALP activity was higher in the O-MSCs and OCS than in the U-MSCs group ($p < 0.05$; Figure 1.3). After staining with ARS, calcium-rich granules were clearly visible in the O-MSCs group, whereas no nodules were observed in the U-MSCs and OCS groups (Figure 1.4.A). The degree of ARS staining was also greater in the O-MSCs group (Figure 1.4.B).

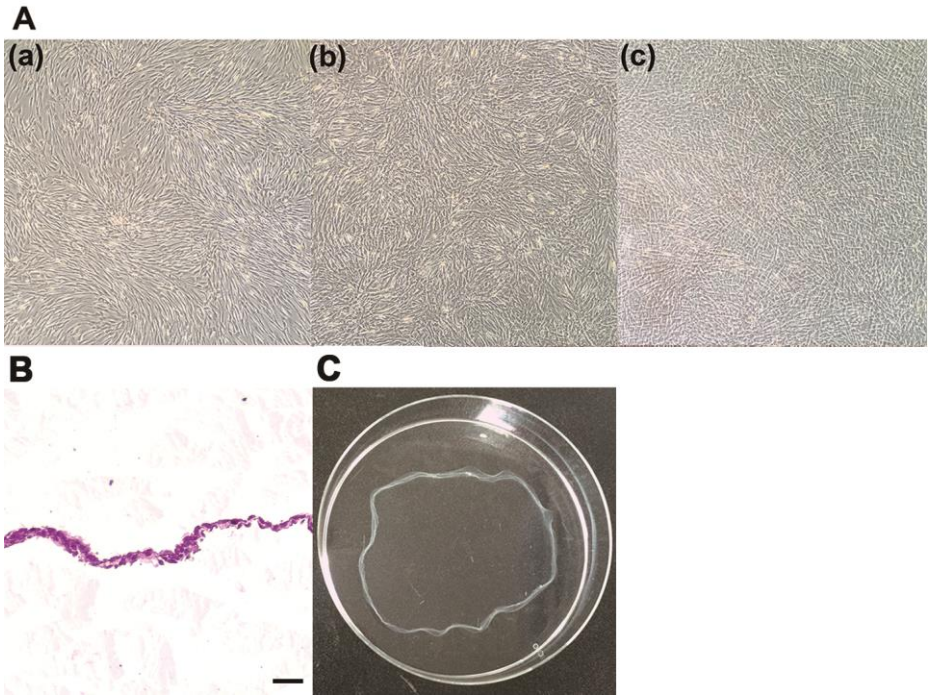

Figure 1.2. Morphological characteristics of the adipose-derived mesenchymal stem cells (Ad-MSCs) and Ad-MSC sheets. (A) a. undifferentiated Ad-MSCs, b. osteogenic Ad-MSCs, c. osteogenic Ad-MSC sheets observed under a phase contrast microscope. (B) OCS was composed of multiple layers of cells surrounded by ECM. (C) OCS was easily detached by cell scraper. Scale bars = 25 μm

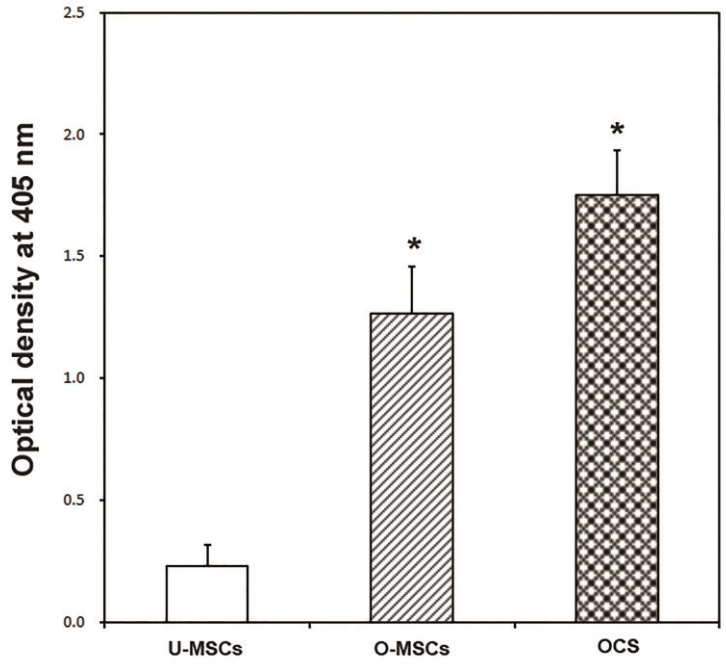

Figure 1.3. Quantification of alkaline phosphatase (ALP) activity. ALP activity was significantly higher in the O-MSCs and OCS than in the U-MSCs group (*$p < 0.05$).

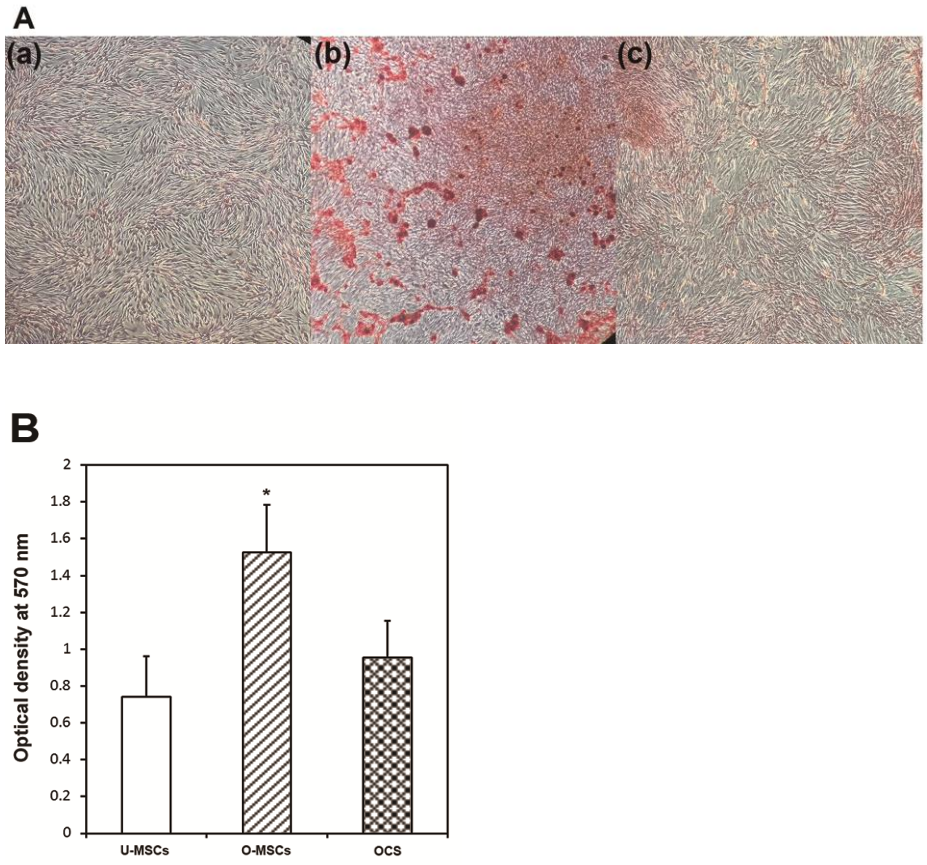

Figure 1.4. Arizarin Red S (ARS) staining. (A) a. U-MSCs, b. O-MSCs, c. OCS were stained using ARS solution. Calcium-rich granules were clearly visible in the O-MSCs group. (B) The degree of mineralization was greater in the O-MSCs group (*$p < 0.05$).

2. Expression of Osteogenic Differentiation Markers in Ad-MSCs and Matrix Cell Sheets

The expression of *runt-related transcription factor 2 (RUNX2), ALP, osteopontin, bone morphogenetic protein 7 (BMP-7),* and *transforming growth factor beta (TGF-β)* mRNA was significantly upregulated in O-MSCs and OCS compared to the U-MSCs control ($p < 0.05$, Figure 1.5). *RUNX2* and *TGF-β* transcript levels were higher in OCS than in the O-MSCs group ($p < 0.05$). The involvement of the Wnt/β-catenin signaling pathway was investigated by evaluating *axis inhibition protein 2 (AXIN2)* and *β-catenin* expression. Both transcripts were upregulated in O-MSCs and OCS relative to U-MSCs ($p < 0.05$). The mRNA level of *vascular endothelial growth factor (VEGF)* tend to be downregulated in O-MSCs and OCS as compared to the U-MSCs group.

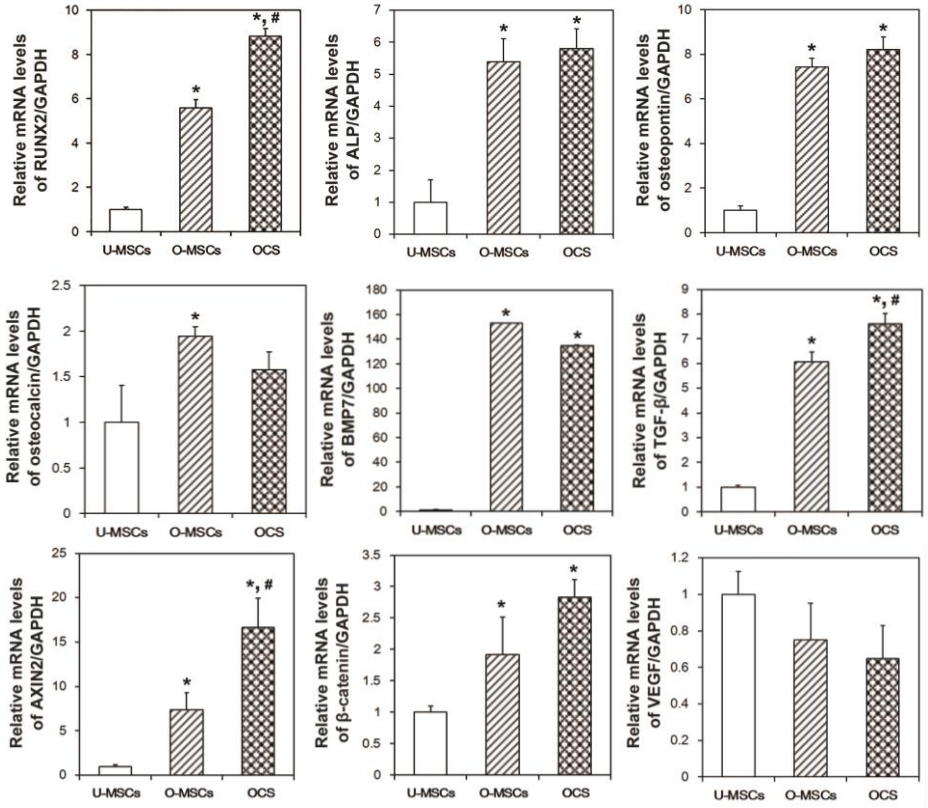

Figure 1.5. Expression of osteogenic differentiation markers. The expression of *RUNX2*, *ALP*, *osteopontin*, *BMP-7*, and *TGF-β* mRNA was significantly upregulated in O-MSCs and OCS (*$p < 0.05$). *RUNX2* and *TGF-β* transcript levels were higher in OCS than in the O-MSCs group (#$p < 0.05$). The *AXIN2* and *β-catenin* mRNA expression was upregulated in O-MSCs and OCS (*$p < 0.05$). *: compared to the U-MSCs group, #: compared to the O-MSCs group.

3. *In vivo* Bone Regeneration in Canine Radial Defects

New bone was detected within defects at the bone margin. In the 3-D reconstructed image, the cone-shaped newly formed bone was visible (Figure 1.6.A). From the sagittal view, the bone volume was discernible (Figure 1.6.B), and a quantitative 3-D micro-CT analysis revealed the following values for newly formed bone mass: PCL/β-TCP, 1.89 ± 1.27 cm^3; PCL/β-TCP/U-MSC, 8.10 ± 1.46 cm^3; PCL/β-TCP/O-MSC, 16.81 ± 3.15 cm^3; PCL/β-TCP/OCS, 26.53 ± 6.02 cm^3; and PCL/β-TCP/O-MSC/OCS, 28.11 ± 5.5 cm^3 (Figure 1.6.C). The amount of new bone formed was greater in all experimental groups than in the PCL/β-TCP group ($p < 0.05$). Moreover, groups with cell sheets (with or without O-MSCs) showed a greater volume of newly formed bone than the other groups ($p < 0.05$).

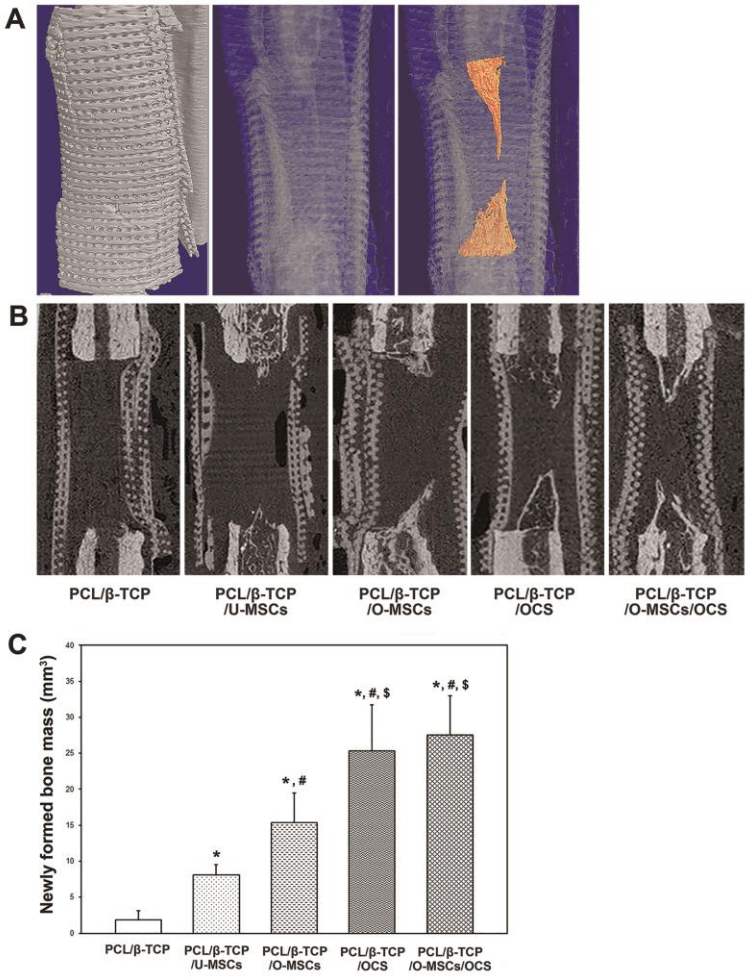

Figure 1.6. Bone regeneration in canine radial defects. (A) 3-D reconstructed image and (B) sagittal view image showed that new bone formation was detected within defects at the bone margin. (C) Quantitative 3-D micro-CT analysis revealed that groups with cell sheets (with or without O-MSCs) showed a greater volume of newly formed bone than the other groups (*, #, $ $p < .05$). *: compared to the PCL/β-TCP group, #: compared to the PCL/β-TCP/U-MSCs group, $: compared to the PCL/β-TCP/O-MSCs group.

4. Histological Evaluation

At 12 weeks after implantation, decalcified paraffin sections were stained with H&E and Masson's trichrome to identify regenerated bone with in defects. In all experimental groups, new bone was observed in longitudinal sections throughout the segmental defect and there was no obvious inflammation. Most of the defect areas were filled with fibrous connective tissue and newly formed bone tissue had a woven, trabecular appearance (Figure 1.7.A). The Masson's trichrome staining revealed abundant collagenous tissue around the regenerated tissue (Figure 1.7.B.a). In addition, vasculatures were observed inside and around the new bone (Figure 1.7.B.b).

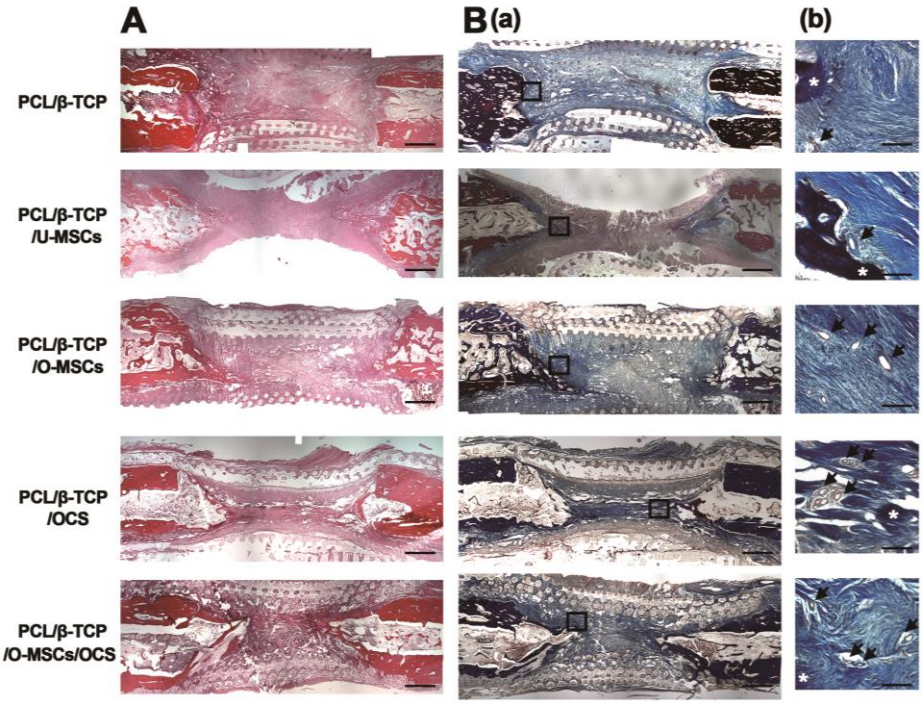

Figure 1.7. Histological analysis. (A) In hematoxylin and eosin staining, most of the defect areas were filled with fibrous connective tissue and newly formed bone tissue had a woven, trabecular appearance. (B) The Masson's trichrome staining revealed abundant collagenous tissue around the regenerated tissue. Vasculatures were observed inside and around the new bone. Asterisks and arrows indicated bone tissue and vasculatures, respectively. Scale bars = (A, B.a) 200 μm, (B.b) 15 μm.

DISCUSSION

The present study investigated the osteogenic potential of Ad-MSCs and Ad-MSC sheets, as well as that of composite PCL/β-TCP scaffolds seeded with Ad-MSCs or wrapped with OCS after their transplantation into critical-sized bone defects in dogs. MSCs have been reported to promote fracture repair; however, injection of single-cell suspensions leads to uneven distribution and weak adhesion of cells, which may ultimate result in cell death (Yamato and Okano, 2004). Additionally, the transplantation of isolated cells is impractical for bone regeneration in large-sized defects, which would require an adequate supply of cells. This is provided by cell sheets, which have intact cell-cell junctions and ECM that confer mechanical support and thereby maintain the integrity of the transplant (Xie *et al.,* 2015). In this study, a cell sheet was created using A2-P; the OCS had multiple layers of proliferating cells with ECM formation. A2-P is a stable form of ascorbic acid that plays a role in collagen biosynthesis and ECM deposition (Yu *et al.,* 2014). The OCS was readily detached from the culture dish using a scraper rather than a proteolytic agent such as trypsin, which preserved critical cell surface proteins such as ion channels, growth factor receptors, and cell-to-cell junction proteins.

MSCs are capable of producing multiple mesenchymal cell lineages under specific culture conditions (Kang *et al.,* 2012; Neupane *et al.,* 2008).

Differentiation into the osteoblastic lineage is induced by culturing in osteoinductive medium containing dexamethasone, vitamin C, and β-glycerophosphate. In this study, the O-MSCs and OCS showed strong osteogenic potential, as evidenced by upregulation of the osteogenic differentiation markers such as *RUNX2*, *ALP*, and *osteopontin* as well as the increased in ALP activity relative to undifferentiated Ad-MSCs. These osteogenic effects of O-MSCs and OCS correspond well with those previously reported (Akahane *et al.,* 2010; Nakamura *et al.,* 2010). In this *in vivo* study, the PCL/β-TCP/O-MSC group showed more extensive bone regeneration than the PCL/β-TCP/U-MSC group, likely due to the higher osteogenic potential of O-MSCs relative to U-MSCs. Moreover, there was more newly formed bone in the PCL/β-TCP/OCS and PCL/β-TCP/O-MSC/OCS groups than in those without OCS. The enhanced bone formation might be due to the delivery of osteogenic cells and ECM to the defected sites by MSC sheets.

As for the role of MSCs in bone tissue engineering, besides osteogenic differentiation, MSCs are thought to exert therapeutic effects via secretion of trophic factors that provide a supportive microenvironment for cell survival, renewal, and differentiation. It has been suggested that wrapped cell sheets function as a tissue-engineered periosteum at bone defect sites. A biomimetic periosteum can maintain homeostasis of the cellular microenvironment by delivering growth factors. Previous study showed that paracrine factors of

MSCs play a positive role in bone repair (Byeon *et al.,* 2010). During bone healing, the proliferation and osteoblastic differentiation of endogenous or exogenous MSCs are influenced by various growth factors, among which TGF-β and BMPs play a major role. Both are members of the TGF-β superfamily, a group of dimeric proteins, acting as growth and differentiation factors. The BMP/TGF-β signaling induces MSCs differentiation into osteoblast via activation of intracellular pathways such as SMAD, mitogen-activated protein kinase signaling (Chen *et al*., 2012; Vanhatupa *et al*., 2015). Wnt signaling is also crucial in bone regeneration. Wnt/β-catenin signaling pathway promotes osteoblastogenesis, activation of osteoblast activity, inhibition of osteoclast activity, and increase bone mass (Guan *et al.,* 2015; Reya and Clevers, 2005). In the present study, OCS showed higher expression of *BMP-7*, *TGF-β*, *AXIN2,* and *β-catenin*, suggesting that the induction of bone regeneration by OCS occurs via activation of the BMP/ TGF-β and Wnt signal pathways.

Osteogenesis requires a well-developed vascular supply. It has been proposed that MSCs and cell sheets stimulate bone formation by inducing vascularization (Akahane *et al.,* 2008; Kang *et al.,* 2012; Nakamura *et al.,* 2010). Neovascularization helps to overcome the hypoxic environment and facilitate bone formation. VEGF promotes angiogenesis and indirectly stimulates bone formation by inducing the ingress of osteoprogenitor cells. In the present study, U-MSCs, O-MSCs, and OCS expressed *VEGF*, which

corresponded to the formation of a vascular network around newly formed bone tissue following transplantation of scaffolds into bone defects. These neovascularization may also have positive effects on the bone tissue regeneration.

In this study, a PCL/β-TCP composite were used as a scaffold for bone regeneration. PCL is a biodegradable polymer with a porous 3-D structure (Yun *et al.,* 2011). This scaffold has approximately 500 μm-sized pores and 70% of porosity, thus it has large surface area. Ceramic powders such as β-TCP, which is an inorganic component of bone, may enhance the mechanical properties of the PCL scaffolds. Recent studies have shown that β-TCP has good osteoconductivity and biocompatibility and promotes MSCs adherence, survival, and osteogenic differentiation (Marino *et al.,* 2010; Muller *et al.,* 2008). Thus, in large bone defects, the PCL/β-TCP composite may provide structural, mechanical support and enhance interactions between scaffold and cells or cell sheets in a manner that is conducive to bone regeneration.

It was demonstrated that osteogenic Ad-MSC sheets have strong osteogenic potential. Moreover, OCS combined with a PCL/β-TCP composite scaffold stimulated new bone formation to repair critical-sized bone defects in dogs. Ad-MSC sheets not only deliver osteogenic cells along with ECM, but also secrete trophic factors at defect sites for the bone regeneration. These findings indicate that the PCL/β-TCP/OCS composite has therapeutic potential for the treatment of bone defects and could be used to improve current treatment

practices.

CHAPTER II

Osteogenic Potential of Adipose-Derived Mesenchymal Stem Cell Sheets Overexpressing BMP-7 in Canine Bone Defects

ABSTRACT

Successful repair of bone defect injuries are a major issue in reconstructive surgery. Multipotent mesenchymal stem cells (MSCs) have potential for bone regeneration. In additions, bone morphogenetic protein 7 (BMP-7) has been shown to possess strong osteoinductive properties. The aim of this study was to investigate the *in vitro* osteogenic capacity of adipose-derived MSC (Ad-MSC) sheets overexpressing BMP-7. In addition, Ad-MSC sheets overexpressing BMP-7 (BMP-7-CS) were transplanted into critical-sized bone defects in dogs and osteogenesis was assessed.

BMP-7 gene expressing lentivirus particles were transduced into Ad-MSCs. Ad-MSCs overexpressing BMP-7 (BMP-7-MSCs) were analyzed by quantitative polymerase chain reaction (qPCR) and western blotting. Ad-MSCs and BMP-7-MSCs were cultured in medium containing ascorbic acid

phosphate to create a cell sheet. After 10 days of *in vitro* culture, the osteogenic capacity was evaluated using alkaline phosphatase (ALP) activity assays and qPCR. BMP-7-CS and BMP-7-CS combined with DBM were transplanted into critical-sized bone defects. The samples were harvested 12 weeks after transplantation, and newly formed bone mass was measured by micro-computed tomography, and histopathological analysis was performed.

BMP-7, at the mRNA and protein level, was up-regulated in BMP-7-MSCs compared to expression in Ad-MSCs. ALP activity in Ad-MSC sheets and BMP-7-CS were significantly higher than that of Ad-MSCs. *ALP, runt related transcription factor 2, osteopontin, BMP-7, transforming growth factor-β, and platelet-derived growth factor* mRNA levels up-regulated in BMP-7-CS compared to expression in Ad-MSCs and Ad-MSC sheets. In a segmental bone defect model, newly formed bone and neovascularization were greater in BMP-7-CS, combination of BMP-7-CS and DBM, compared to those in control group.

These results demonstrate that lentiviral-mediated gene transfer of BMP-7 into Ad-MSCs allows for stable BMP-7 production. BMP-7-CS reveals higher osteogenic capacity than that of Ad-MSCs and Ad-MSC sheets. In addition, BMP-7-CS combined with DBM stimulated new bone and blood vessel formation in a canine critical-sized bone defect. The BMP-7-CS not only provides BMP-7 producing MSCs but also produce osteogenic and vascular trophic factors. The combination of these cells with the osteoinduction and

osteoconduction properties of DBM could result in synergy during bone regeneration. Thus, BMP-7-CS and DBM has therapeutic potential for the treatment of critical-sized bone defects and this could be used to further enhance clinical outcomes during bone defects treatment.

INTRODUCTION

Trauma, tumor resection, and skeletal abnormalities are the main reasons for large bone defects. Successful repair of bone defect injuries are a major issue in reconstructive surgery. Autologous bone tissue transplantation is considered the most appropriate technique to treat large bone defects; however, this method has several drawbacks, including donor site morbidity, chronic pain, and inadequate volume of graft material (Cancedda *et al.*, 2007).

To preclude these problems, bone tissue engineering using stem cells has been developed as an alternative strategy of bone graft. In particular, mesenchymal stem cells (MSCs) show great potential for therapeutic use in bone tissue engineering due to their capacity for osteogenic differentiation and regeneration (Kang *et al.,* 2012). Cell sheets are beneficial for cell transplantation because cell-cell junctions and endogenous extracellular matrix (ECM) are preserved, thereby ensuring homeostasis of the cellular microenvironment for the delivery of growth factors and cytokines that promote the tissue repair over a prolonged period of time (Akahane *et al.*, 2008; Long *et al.*, 2014).

Osteoblast differentiation from multipotent stem cells is regulated by bone morphogenetic proteins (BMPs), which are members of the transforming growth factor (TGF) superfamily. Many studies have demonstrated that recombinant BMPs can stimulate bone formation (Alaee *et al.*, 2014; Cook *et*

al., 1994; Wang *et al.,* 1990). However, large doses of recombinant BMP are required to produce an adequate biological response and it is quite expensive. The development of gene-modified tissue engineering is an attractive approach with great potential for repairing bone defects. Lentiviral-based gene therapy systems offer prolonged gene expression, and might be ideal for the treatment of large bone defects that require a long-term osteoinductive stimulus or in cases wherein the host biological environment has been compromised (Hsu *et al.,* 2007; Sugiyama *et al.,* 2005).

Among bone substitutes, demineralized bone matrix (DBM) is effective and widely used clinically. DBM is prepared by acid extraction from allograft bone. This process exposes BMPs and other peptide-signaling molecules on the retained collagen skeleton to improve the osteoinductive and osteoconductive potential (Mauney *et al.,* 2005). Growth factors such as insulin-like growth factor-1 and TGF-β have also been identified in DBM (Wildemann *et al.,* 2007). Therefore, the DBM has become a suitable alternative to autologous bone grafts in certain clinical situations such as bone defects and comminuted fracture with bone loss.

Osteogenesis, osteoinduction, and osteoconduction are considered important for bone regeneration; therefore, treatment strategies should include all prerequisites of optimal bone healing, such as osteogenic cells, osteoconductive matrix, and osteoinductive factors. I hypothesized that combining MSC sheets and DBM could accelerate and enhance bone

regeneration in large bone defects.

In this study, canine adipose-derived MSCs (Ad-MSCs) overexpressing BMP-7 were produced and cell sheets were generated. The osteogenic potentials of Ad-MSC sheets and Ad-MSC sheets overexpressing BMP-7 (BMP-7-CS) were compared *in vitro*. In addition, BMP-7-CS, with or without DBM particles, were constructed and assessed for their *in vivo* osteogenic potential after transplantation into critical-sized bone defects in dogs.

MATERIALS AND METHODS

1. Isolation and culture of canine Ad-MSCs

The study protocol was approved by the Institutional Animal Care and Use Committee of Seoul National University (SNU-150624-7). MSCs derived from canine hip adipose tissue were isolated and characterized (Ryu *et al.*, 2009). The tissue was collected aseptically from the subcutaneous fat of a 2-year-old beagle dog under anesthesia, and washed with Dulbecco's phosphate-buffered saline (DPBS; Thermo Fisher Scientific Inc., USA), minced, then digested with collagenase type I (1 mg/ml; Sigma-Aldrich, USA) at 37℃ for 30–60 minutes with intermittent shaking. The suspension was filtered through a 100-μm nylon mesh and centrifuged to separate floating adipocytes from stromal cells. Pre-adipocytes in the stromal vascular fraction were plated at 8,000–10,000 cells/cm^2 in T175 culture flasks containing Dulbecco's modified Eagle's medium (Thermo Fisher Scientific Inc.) supplemented with 3.7 g/l sodium bicarbonate, 1% penicillin/streptomycin, 1.7 mM L-glutamine, and 10% fetal bovine serum (Thermo Fisher Scientific Inc.). Cells were incubated in a humidified atmosphere at 37℃ and 5% CO_2. Unattached cells and residual non-adherent red blood cells were removed after 24 hours by washing with PBS, and the culture medium was replaced every 2 days. Cells

were used for experiments after the third passage.

2. Lentiviral packing and transduction

The canine *BMP-7* gene was cloned in reference to the gene database. A lentiviral vector encoding BMP-7 and green fluorescent protein (GFP) cDNA downstream of the elongation factor-1 alpha promoter was constructed (Figure 2.1). Twenty-four hours before transfection, 4×10^6 HEK293T cells were seeded in a 100-mm dish. The following day, a lentiviral packaging mix (System Biosciences, USA) and lentiviral transgene plasmids were transfected into each well to create lentivirus. Virus particles were collected and transduced into Ad-MSCs at passage one. After Ad-MSCs reached 90% confluence, the stable cells were selected using puromycin (3 μg/ml, Thermo Fisher Scientific Inc.). Ad-MSCs were subcultured, and passage three cells were used for the following experiments.

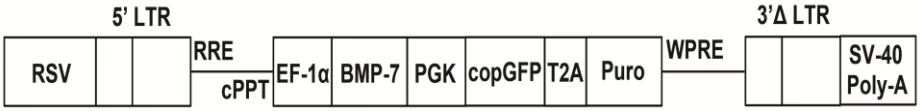

Figure 2.1. Construction of lentiviral vector. Lentiviral vectors contain an EF-1α promoter, BMP-7, copGFP, and puromycin genes. RSV: Rous sarcoma virus U3, LTR: long terminal repeat, RRE: Rev-responsible element, cPPT: central polyprine tract, WPRE: woodchuck hepatitis virus post-transcriptional regulatory element

3. *In vitro* BMP-7 quantification

3.1. Gene expression analysis for identification of BMP-7 overexpression

Total RNA was isolated from Ad-MSCs or Ad-MSCs overexpressing BMP-7 (BMP-7-MSCs) using the Hybrid-RTM RNA extraction kit (GeneAll Bio, Korea) according to the manufacturer's protocol. RNA concentration was determined by measuring optical density at 260 nm with a NanoDrop ND-1000 spectrophotometer (Nano Drop Technologies, USA). cDNA was synthesized from RNA using a commercially available cDNA synthesis kit (Takara Bio Inc., Japan). Quantitative reverse transcription polymerase chain reaction (qRT-PCR) was performed with an ABI 7300 Real-time-PCR system (Applied Biosystems, USA), using SYBR Premix Ex Taq (Takara Bio Inc.). *BMP-7* primer sequences are listed in Table 1. Expression levels of target genes were normalized to the level of glyceraldehyde 3-phosphate dehydrogenase (GAPDH), and quantitated using the ΔΔCt method (Livak and Schmittgen, 2001).

Table 2.1. Primers sequences used for quantitative reverse transcription PCR

Target gene		**Primer sequence (5'-3')**
RUNX2	Forward	TGTCATGGCGGGTAACGAT
	Reverse	TCCGGCCCACAAATCTCA
ALP	Forward	TCCGAGATGGTGGAAATAGC
	Reverse	GGGCCAGACCAAAGATAGAG
Osteopontin	Forward	GATGATGGAGACGATGTGGATA
	Reverse	TGGAATGTCAGTGGGAAAATC
Osteocalcin	Forward	CTGGTCCAGCAGATGCAAAG
	Reverse	GGTCAGCCAGCTCGTCACAGTT
BMP-7	Forward	TCGTGGAGCATGACAAAGAG
	Reverse	GCTCCCGAATGTAGTCCTTG
TGF-β	Forward	CTCAGTGCCCACTGTTCCTG
	Reverse	TCCGTGGAGCTGAAGCAGTA
VEGF	Forward	CTATGGCAGGAGGAGAGCAC
	Reverse	GCTGCAGGAAACTCATCTCC
PDGF-β	Forward	CCGAGGAGCTCTACGAGATG
	Reverse	AACTCTCCAGCTCGTCTCCA
GAPDH	Forward	CATTGCCCTCAATGACCACT
	Reverse	TCCTTGGAGGCCATGTAGAC

3.2. Protein expression analysis for identification of BMP-7 overexpression

Ad-MSCs and BMP-7-MSCs were used for western blot analysis. Briefly, the cells were washed twice with DPBS, and sonicated in lysis buffer (150 mM sodium chloride, 1% Triton X-100, 1% sodium deoxycholate, 0.1% sodium dodecyl sulfate (SDS), 50 mM Tris at pH 7.5, 2 mM EDTA) on ice for 30 minutes. Lysates were cleared by centrifugation (10 minutes at 13000 × *g* and 4℃), and protein concentrations were determined using the Bradford method (Bradford 1976). Equal amounts of protein (15 μg) were resolved by electrophoresis on 10% SDS-polyacrylamide gels and transferred to polyvinylidene fluoride membranes. Membrane blots were washed with TBST (10 mM Tris-HCl, pH 7.6, 150 mM NaCl, 0.05% Tween-20), blocked with 5% skim milk for 1 hour, and incubated with the appropriate primary antibodies at the recommended dilutions. The antibodies used included antibodies against actin (A3853, Sigma-Aldrich), BMP-7 (ab56023, Abcam). The primary antibodies (1:1000) were diluted in TBST. The membrane was then washed, and primary antibodies were detected with goat anti-rabbit IgG or goat anti-mouse IgG conjugated to horseradish peroxidase (1:5000, Invitrogen, USA). Bands were visualized using enhanced chemiluminescence (Invitrogen).

4. Preparation of Ad-MSC sheets and BMP-7-CS

Ad-MSC sheets and BMP-7-CS were prepared as previously described (Akahane *et al.,* 2008). Briefly, Ad-MSCs and BMP-7-MSCs were seeded at a density of 1×10^4 cells/cm^2 in a 100-mm culture dish and cultured in growth medium containing 82 μg/ml L-ascorbic acid 2-phosphate (Sigma-Aldrich) for 10 days. Ad-MSCs (negative control) were cultured in unsupplemented growth medium for 10 days.

5. Gene expression analysis

The expression of osteogenic differentiation markers and vascular-related markers was investigated on day 10. Total RNA was isolated from cells or cell sheets and qRT-PCR was performed as previously mentioned. Primer sequences are listed in Table 2.1.

6. Alkaline phosphatase (ALP) activity measurement

Cells cultured in 100-mm dishes were used for the measurement of ALP activity using an ALP assay kit (Takara Bio Inc.) according to the manufacturer's instructions. Briefly, p-nitrophenyl phosphate (pNPP) solution

was prepared by dissolving 24 mg pNPP substrate in 5 ml ALP buffer. Cells were scraped into 200 μl of extraction solution, homogenized, and sonicated. The cleared supernatant was collected after centrifugation at 13000 × *g* at 4℃ for 10 minutes. A 50-μl volume of cell lysate supernatant was mixed with 50 μl of pNPP substrate solution and incubated at 37℃ for 30 minutes. After adding 50 μl of stop solution (0.5N NaOH), absorbance was measured at 405 nm with a spectrophotometer.

7. Fabrication of PCL/β-TCP scaffolds

Poly ε-caprolactone (PCL) was dissolved in chloroform at 40℃. NaCl and β-tricalcium phosphate (β-TCP) were ground and sieved, and granules between 25 and 33 μm were selected. β-TCP was prepared by calcination of nano-TCP (Merck, USA) at 1,000℃ for 4 hours. Selected NaCl granules were mixed with predetermined amounts of ceramic particles (1:1 = NaCl:PCL, 1.5:1 = ceramic:PCL, weight ratios). Combined powders were mixed with the PCL suspension to produce a homogeneous paste. Sheet-type porous scaffolds (50 × 25 × 2 mm) were constructed by extruding the gel paste onto a substrate using a three-dimensional (3-D) printing system. The shapes and sizes of the PCL/β-TCP scaffolds were designed using a computer system. NaCl was removed by immersing the scaffold in deionized water to produce macro-

sized pores in strut and the water was replaced every 2 hours with fresh water at 30℃ after sufficient drying of the scaffold.

8. Animal experiments

Beagle dogs (n = 12; 2–3 years old) weighing 9.1 ± 1.6 kg were used for this study. Dogs were handled in accordance with the animal care guidelines of the Institute of Laboratory Animal Resources, Seoul National University, Korea. The dogs were assigned to one of three groups (n = 4 for each group), including control, BMP-7-CS, and BMP-7-CS/DBM. For all groups, the defects were surrounded with PCL/β-TCP. For the BMP-7-CS group, PCL/β-TCP was wrapped with four BMP-7-CS after 10 days of culture. Additionally, DBM particles (Veterinary tissue bank, UK) were placed in the defects for the BMP-7-CS/DBM group. The Institutional Animal Care and Use Committee of Seoul National University approved the experimental design. Dogs were medicated and anesthetized with tramadol (4 mg/kg by intravenous (i.v.) injection; Toranzin; Samsung Pharmaceutical Co., Korea), propofol (6 mg/kg i.v.; Provive; Claris Lifesciences, Indonesia), and atropine sulfate (0.05 mg/kg by subcutaneous injection; Jeil Pharmaceutical Co., Korea). Anesthesia was maintained with isoflurane (Forane solution; Choongwae Pharmaceutical Co., Korea) at a 1.5 minimum alveolar concentration throughout the procedure.

Electrocardiography, pulse oximetry, respiratory gas analysis, and rectal temperature measurement were performed using an anesthetic monitoring system (Datex-Ohmeda S/5; GE Healthcare, UK). Under sterile conditions, a craniomedial incision was made in the skin to expose the diaphysis of the left radius. A 15 mm-long segmental defect was made in the middle portion of the diaphysis using an oscillating saw (Stryker, USA). Defects were surrounded by the experimental scaffold and filled with and without DBM. A nine-hole, 2.7-mm dynamic compression plate (DePuy Synthes, Switzerland) was placed on the cranial aspect of the radius. The soft tissue was closed with 3-0 polydioxanone sutures (Ethicon, USA), and the skin was closed with 4-0 nylon sutures.

9. Micro-computed tomography (CT) for bone imaging

Dogs were sacrificed 12 weeks after implantation. The radius segment was excised, trimmed, and fixed in 10% formaldehyde. Samples were scanned using a micro-CT system (Skyscan; Bruker Corp., Belgium) and 3-D images were reconstructed; the volume of newly formed bone, within bone defects, was calculated using the auxiliary software (Bruker Corp.).

10. Histological analysis

After micro-CT measurements, specimens were decalcified in 8% nitric acid for 2 weeks at room temperature, dehydrated using a graded series of alcohol, embedded in paraffin, sectioned at a thickness of 5 μm, and stained with hematoxylin and eosin (H&E) or Masson's trichrome according to standard protocols. For the tracking of BMP-7-CS expressing GFP, the tissue was stained with 4'6-diamidino-2-phenylindole (DAPI, 1:100, Sigma-Aldrich) to identify nuclei and observed under a fluorescence microscope (Life technologies, USA).

11. Statistical analysis

Results are expressed as the mean ± standard deviation. Statistical analysis was performed using SPSS v.22.0 software (IBM Corp., USA). Group means were compared using Kruskal-Wallis tests followed by Mann-Whitney U tests. A p value of less than 0.05 was considered statistically significant.

RESULTS

1. Gene transduction and BMP-7 production *In vitro*

Canine Ad-MSCs were transduced with lentiviral vector encoding the *GFP* and *BMP-7* gene. GFP-expressing BMP-7-MSCs was identified after transduction. The expression of *BMP-7* mRNA and BMP-7 protein was significantly upregulated in BMP-7-MSCs compared to that of Ad-MSCs ($p < 0.05$, Figure. 2.2).

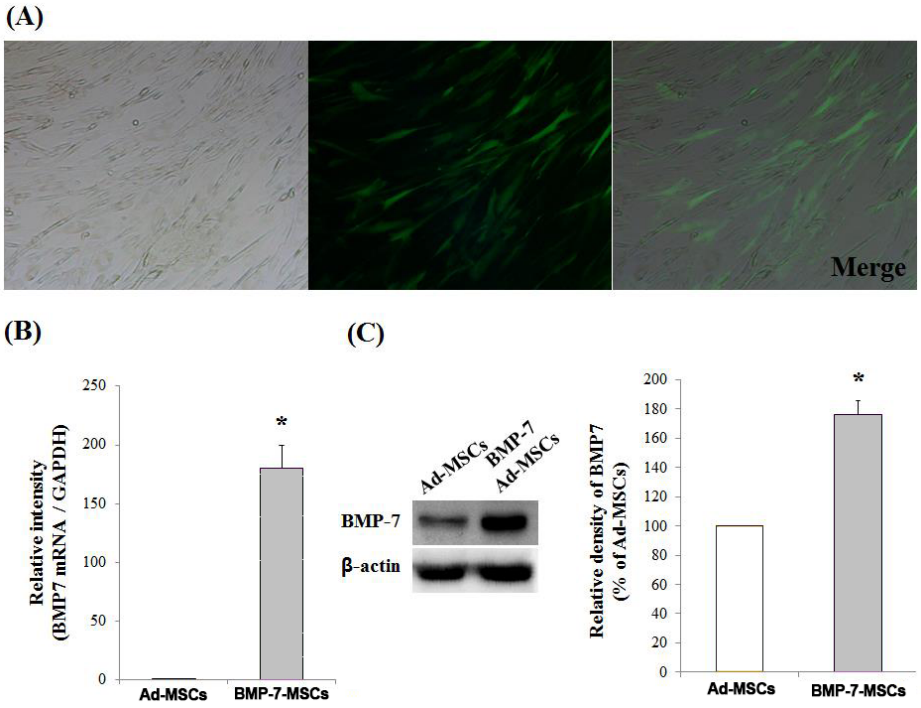

Figure 2.2. (A) Green fluorescence protein was observed in Ad-MSCs after lentivirus transduction. (B) *BMP-7* mRNA levels in BMP-7-MSCs were up-regulated compared to that of Ad-MSCs (*$p < 0.05$). (C) BMP-7 protein expression in BMP-7-MSCs was higher than in Ad-MSCs (*$p < 0.05$).

2. ALP activity

The ALP activity of each group was assessed at 10 days after changing cell sheet medium. The ALP activity was enhanced 6.4-fold and 7.8-fold in Ad-MSC sheets and the BMP-7-CS group, respectively compared to that of the Ad-MSCs control group ($p < 0.05$, Figure 2.3).

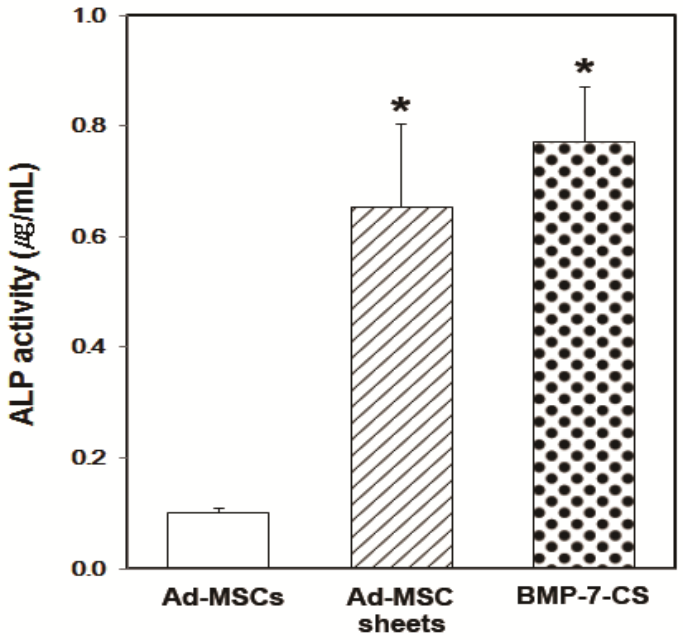

Figure 2.3. Quantification of alkaline phosphatase (ALP) activity. ALP activity was significantly higher in the Ad-MSC sheets and BMP-7-CS than in the Ad-MSCs group (*$p < 0.05$).

3. Real-time quantitative PCR analysis

The expression of *runt-related transcription factor 2 (RUNX2), ALP, osteopontin, osteocalcin, BMP-7* and *TGF-β* mRNA was significantly upregulated in Ad-MSC sheets and BMP-7-CS compared to that of Ad-MSCs control ($p < 0.05$, Figure 2.4). The transcript levels of almost all osteogenic differentiation markers were higher in the BMP-7-CS group than in the Ad-MSC sheets group ($p < 0.05$); the exception was the *osteocalcin*. Vascular-related markers were also investigated by evaluating *vascular endothelial growth factor (VEGF)* and *platelet-derived growth factor-β (PDGF-β)* expression. The mRNA level of *VEGF* was not different among the groups. However, *PDGF-β* mRNA was significantly upregulated in Ad-MSC sheets and BMP-7-CS compared to that of Ad-MSCs ($p < 0.05$).

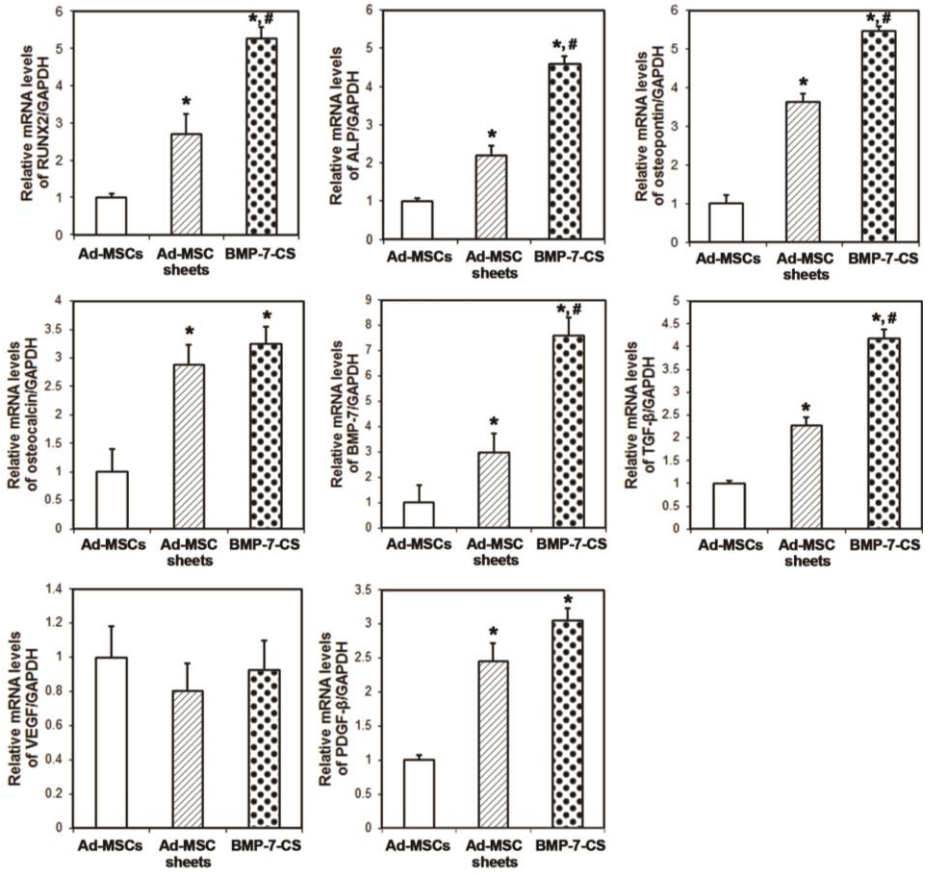

Figure 2.4. Expression of osteogenic differentiation and vascular-related markers. The expression of *RUNX2*, *ALP*, *osteopontin*, *BMP-7*, and *TGF-β* mRNA was significantly upregulated in Ad-MSC sheets and BMP-7-CS compared to that of Ad-MSCs (*$p < 0.05$). Except for *osteocalcin*, transcript levels of osteogenic differentiation markers were higher in BMP-7-CS than in the Ad-MSC sheets group (#$p < 0.05$). *PDGF-β* mRNA expression was upregulated in Ad-MSC sheets and BMP-7-CS (*$p < 0.05$). *: compared to the Ad-MSCs group, #: compared to the Ad-MSC sheets group

4. *In vivo* bone regeneration in canine radial defects

New bone was detected within defects at each bone margin. In the 3-D reconstructed image, the cone-shaped newly formed bone was visible (Figure 2.5.A). From the sagittal view, the bone volume was discernible (Figure 2.5.B), and a quantitative 3-D micro-CT analysis revealed the following values for newly formed bone mass: control, 14.12 ± 5.54 cm^3; BMP-7-CS, 44.37 ± 17.33 cm^3; and BMP-7-CS/DBM, 49.30 ± 16.06 cm^3 (Figure 2.5.C). The amount of new bone formed was greater in BMP-7-CS and BMP-7-CS/DBM groups than in the control group ($p < 0.05$). Moreover, mineralized bone particles were observed in the defect area of the BMP-7-CS/DBM group.

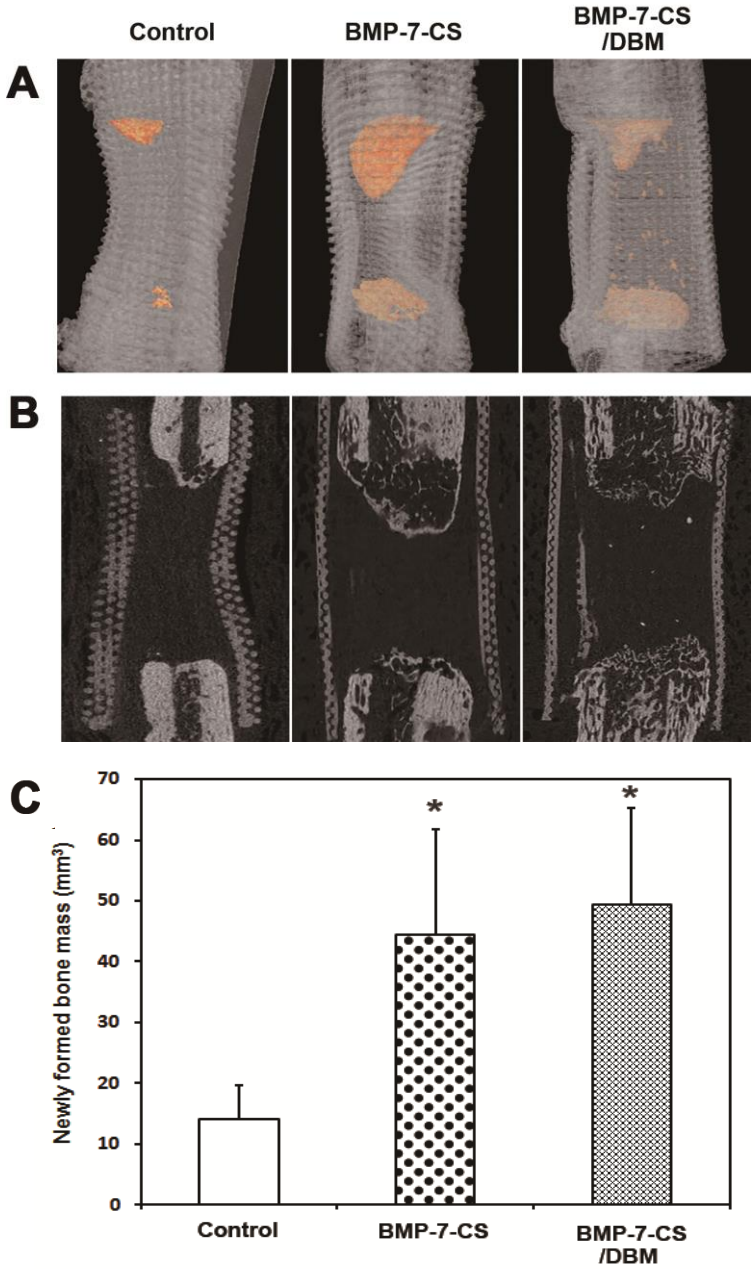
Control
BMP-7-CS
BMP-7-CS /DBM
A
B
C
Newly formed bone mass (mm³)
70
60
50
40
30
20
10
0
*
*
Control
BMP-7-CS
BMP-7-CS /DBM

Figure 2.5. Bone regeneration in canine radial defects. (A) 3-D reconstructed image and (B) sagittal view image showed that new bone formation was detected within defects at the bone margin. Moreover, mineralized bone particles were observed in the defect area of BMP-7-CS/DBM group. (C) Quantitative 3-D micro-CT analysis revealed that groups with BMP-7-CS (with or without DBM) showed a greater volume of newly formed bone than control groups (*$p < 0.05$).

5. Histological evaluation

At 12 weeks after implantation, decalcified paraffin sections were stained by H&E and Masson's trichrome to identify regenerated bone in defects. Newly formed bone was observed in longitudinal sections throughout the segmental defect of all groups (Figure 2.6.A). In the control group, most of the defect areas were filled with fibrous connective tissue with minimal new bone formation. In the BMP-7-CS group, fibrous connective tissue was also observed and newly formed bone tissue had a woven, trabecular appearance. In the BMP-7-CS/DBM group, DBM particles mainly filled the defect and fibrous connective tissue existed among these particles. Masson's trichrome staining revealed abundant collagenous tissue around the regenerated tissue (Figure 2.6.B.a). In addition, vasculature was observed around the new bone and DBM particles (Figure 2.6.B.b). The BMP-7-CS and BMP-7-CS/DBM groups showed enhanced vasculature compared to that of the control group.

To determine the engraftment of BMP-7-MSCs, GFP was examined at 12 weeks after transplantation of BMP-7-CS. GFP labeled BMP-7-MSCs were observed around the new bone and DBM particles (Figure 2.7).

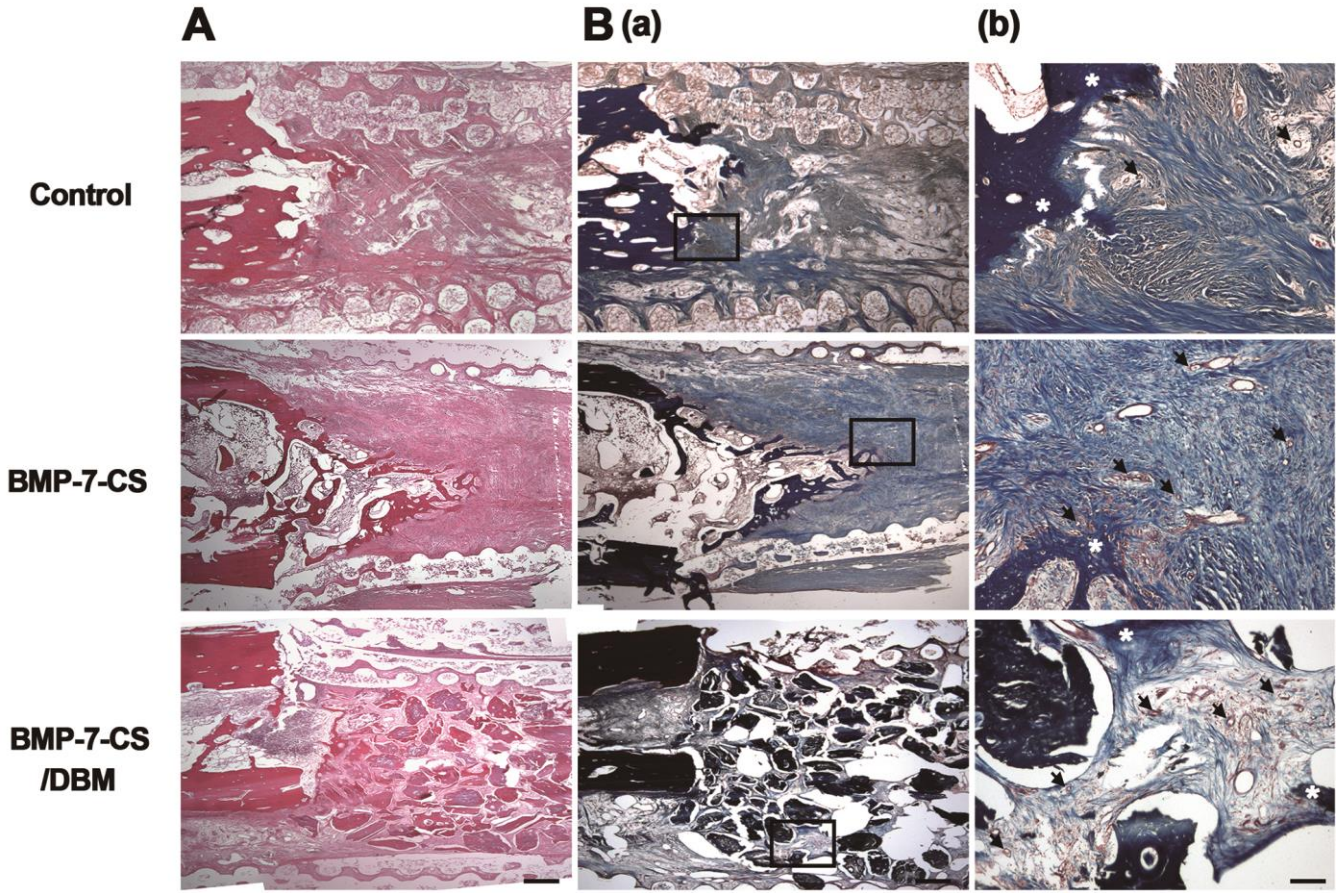
A
B (a)
(b)
Control
BMP-7-CS
BMP-7-CS
/DBM

Figure 2.6. Histological analysis. (A) In H&E staining, most of the defect areas were filled with fibrous connective tissue and newly formed bone tissue had a woven, trabecular appearance. Additionally, the defect site was filled with DBM particles in the BMP-7-CS/DBM group. (B.a) The Masson's trichrome staining revealed abundant collagenous tissue around the regenerated tissue. (B.b) Vasculature was observed around the new bone and DBM particles. Asterisks and arrows indicate bone tissue and vasculatures, respectively. Scale Bar: A,B.a, 250 μm; B.b, 25 μm.

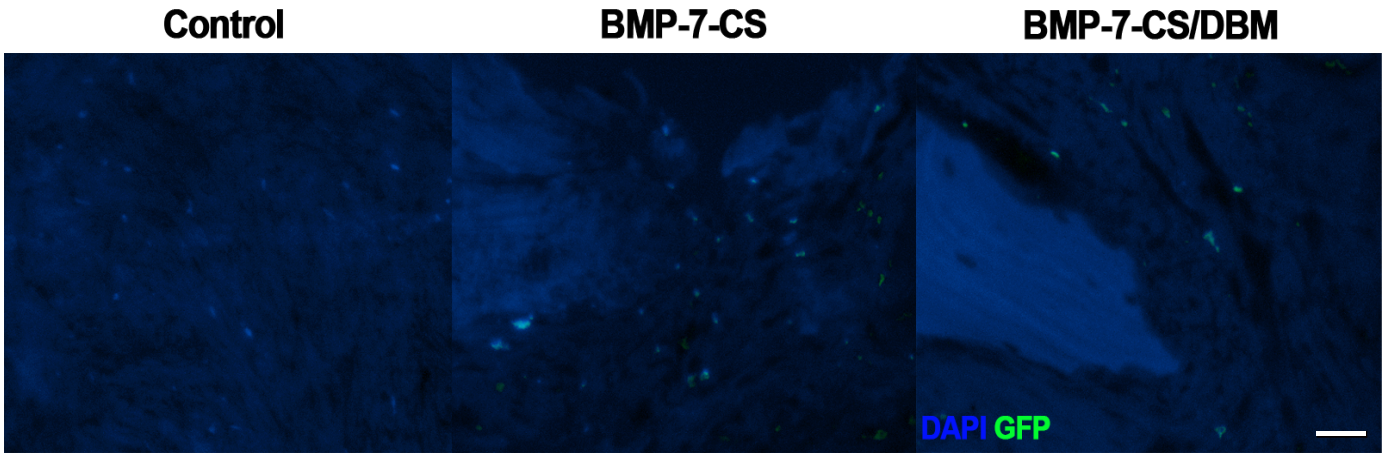

Figure 2.7. GFP expression at 12 weeks after transplantation of BMP-7-CS. GFP labeled BMP-7-MSCs were observed around the new bone and DBM particles. DAPI stains were observed in the nucleus but GFP was not in the control. Scale Bar: 25 μm.

DISCUSSION

The present study investigated the osteogenic potential of BMP-7-CS, as well as BMP-7-CS with and without DBM particles after transplantation into critical-sized bone defects in dogs. The scientific literature provides extensive evidence for the osteoblastic potential of MSCs (Byeon *et al.*, 2010). An adequate supply of MSCs is important for efficient bone regeneration in large bone defects. However, injection of single-cell suspensions leads to uneven distribution and weak cell adhesion, which can ultimately result into cells death (Yamato and Okano 2004). Cell sheet technology has been developed to enhance the regenerative capacity of tissue-engineered products (Akahane *et al.*, 2008; Long *et al.*, 2014). For this methodology, sheets maintain intact cell-cell junctions and ECM. The ECM provides cells with not only structural support to maintain the integrity of the transplant (Xie *et al.*, 2015).

Combination therapies with MSCs and growth factors were investigated to enhance bone repair. Of these growth factors, BMPs have been extensively studied as potent osteoinductive factors (Burastero *et al.*, 2010; Dimitriou *et al.*, 2011). BMPs initiate the bone healing cascade through the recruitment of MSCs from local bone and soft tissues and guide the differentiation of MSCs into osteoblasts. In the present study, a regional lentiviral gene delivery system was used, and successfully transduced the BMP-7 gene into Ad-MSCs.

BMP-7 MSCs secreted more BMP-7 than control Ad-MSCs. Regional gene therapy is a potential treatment option based on the sustained release of growth factors. Previous studies using lentiviral gene therapy demonstrated high levels of expression of BMP proteins for at least 3 months (Hsu *et al.*, 2007; Pensak *et al.*, 2015). Similarly, in this study, transduced cells produced GFP at 12 weeks after transplantation. The longer duration of BMP production associated with the lentiviral vector was responsible for better bone repair in the large bone defects.

In the present study, BMP-7-CS, which was produced from BMP-7-MSCs, showed strong osteogenic potential, as evidenced by upregulation of osteogenic differentiation markers such as *RUNX2, ALP, osteopontin,* and *osteocalcin* as well as by increased ALP activity relative to Ad-MSCs and Ad-MSC sheets. In addition, in this *in vivo* study, the BMP-7-CS group showed more extensive bone regeneration than the control group. During bone healing, the proliferation and osteoblastic differentiation of endogenous or exogenous MSCs are influenced by various growth factors, among which TGF-β and BMPs are important. BMP/TGF-β signaling induces MSCs differentiation into osteoblasts via activation of intracellular pathways such as SMAD and mitogen-activated protein kinase signaling (Chen *et al.,* 2012; Vanhatupa *et al.,* 2015). Overexpression of BMP-7 from implanted MSCs can affect osteogenic differentiation of endogenous and exogenous MSCs. However, the donor cells appeared to function more as a BMP delivery vehicle, as opposed

to differentiating into osteoblasts (Pensak *et al.*, 2015). In addition, it has been suggested that wrapped cell sheets function as a tissue-engineered periosteum at the defected bone segment. A biomimetic periosteum can maintain homeostasis of the cellular microenvironment by delivering growth factors.

The requirements for grafting material are substantial for regeneration in large bone defects. DBM is one such allograft material that has been shown to have osteoinductive and osteoconductive activities (Katz *et al.,* 2009). Early bone formation is related to the osteoconductive capacity of DBM that allows osteoblast precursors to adhere to a collagen matrix similar to endogenous cortical bone matrix (An *et al.*, 2015). Although DBM by itself is believed to enhance bone formation, its osteogenic ability is not sufficient. The tissue-engineering approach is a promising strategy for bone regenerative medicine, with the goal of generating new cell-driven, functional tissues, rather than just implanting non-living scaffolds. In the present study, a high amount of new bone formation and calcium deposition inside the DBM particles was found in the DBM/BMP-7-CS group. Moreover, vascularization around newly formed bone as well as DBM particles was also identified.

Vascularization may have contributed to homeostasis of the microenvironment that promoted cells survival and bone formation. Some reports proposed that MSCs and cell sheets stimulate bone formation by inducing vascularization (Kang *et al.,* 2012; Nakamura *et al.,* 2010). Neovascularization alleviates hypoxia, and is necessary for bone formation.

VEGF and corresponding receptors are key regulators in a cascade of molecular and cellular events that ultimately lead to the development of the vascular system. In the present study, Ad-MSC sheets and BMP-7-CS expressed *VEGF and PDFG-β,* which corresponded to the formation of a vascular network around the newly formed bone tissue following transplantation. Developed vascular beds around DBM particles might be involved in increased mineralization of DBM through osteoblast invasion. Neovascularization and the existence of several mineralized materials might enhance overall bone regeneration in critical-sized bone defects.

It was demonstrated that lentiviral-mediated gene transfer of BMP-7 into Ad-MSCs allows production of BMP-7. The BMP-7-CS also showed strong osteogenic potential. The BMP-7-CS not only provides BMP-7 producing MSCs with ECM but also secrete osteogenic and vascular trophic factors. The combination of these cell sheets with the osteoinduction and osteoconduction properties of DBM could result in synergy during bone regeneration. Combination of BMP-7-CS and DBM has therapeutic potential for the treatment of critical-sized bone defects and this could be used to further enhance clinical outcomes during bone defects treatment.

CONCLUSION

This study was performed to investigate strategy for enhancing bone regeneration effects of various modifications of Ad-MSCs or Ad-MSC sheets. These were compared the osteogenic potentials *in vitro* and also assessed for their *in vivo* osteogenic potentials after transplantation into the critical-sized bone defects. The conclusions are as follows:

1. The OCS could be fabricated and had strong osteogenic potentials *in vitro*.

2. The OCS combined with a PCL/β-TCP composite scaffold stimulated new bone formation to repair critical-sized bone defects.

3. Lentiviral-mediated gene transfer of BMP-7 into Ad-MSCs and allowed for stable BMP-7 production. The BMP-7-CS also showed strong osteogenic potentials *in vitro*.

4. The BMP-7-CS combined with DBM showed more new bone formation and better bone regeneration process to repair critical-sized bone defects.

Overall, combination of the BMP-7-CS and DBM has a potential bone regeneration effect, and it could be used for the treatment of bone defects.

REFERENCES

Akahane M, Nakamura A, Ohgushi H, Shigematsu H, Dohi Y, Takakura Y. Osteogenic matrix sheet-cell transplantation using osteoblastic cell sheet resulted in bone formation without scaffold at an ectopic site. J Tissue Eng Regen Med 2008; 2: 196-201.

Akahane M, Shigematsu H, Tadokoro M, Ueha T, Matsumoto T, Tohma Y, Kido A, Imamura T, Tanaka Y. Scaffold-free cell sheet injection results in bone formation. J Tissue Eng Regen Med 2010; 4: 404-411.

Alaee F, Hong SH, Dukas AG, Pensak MJ, Rowe DW, Lieberman JR. Evaluation of osteogenic cell differentiation in response to bone morphogenetic protein or demineralized bone matrix in a critical sized defect model using GFP reporter mice. J Orthop Res 2014; 32: 1120-1128.

Ali SA, Zhong SP, Doherty PJ, Williams DF. Mechanisms of polymer degradation in implantable devices. I. Poly(caprolactone). Biomaterials 1993; 14: 648-656.

An S, Gao Y, Huang X, Ling J, Liu Z, Xiao Y. A comparative study of the proliferation and osteogenic differentiation of human periodontal ligament cells cultured on beta-TCP ceramics and demineralized bone matrix with or without osteogenic inducers in vitro. Int J Mol Med 2015; 35: 1341-1346.

Bradford MM. A rapid and sensitive method for the quantitation of microgram quantities of protein utilizing the principle of protein-dye binding. Anal Biochem 1976; 72: 248-254.

Burastero G, Scarfi S, Ferraris C, Fresia C, Sessarego N, Fruscione F, Monetti F, Scarfò F, Schupbach P, Podestà M, Grappiolo G, Zocchi E. The association of human mesenchymal stem cells with BMP-7 improves bone regeneration of critical-size segmental bone defects in athymic rats. Bone 2010; 47: 117-126.

Byeon YE, Ryu HH, Park SS, Koyama Y, Kikuchi M, Kim WH, Kang KS, Kweon OK. Paracrine effect of canine allogenic umbilical cord blood-derived mesenchymal stromal cells mixed with beta-tricalcium phosphate on bone regeneration in ectopic implantations. Cytotherapy 2010; 12: 626-636.

Calori GM, Giannoudis PV. Enhancement of fracture healing with the diamond concept: the role of the biological chamber, Injury 2011; 42: 1191-1193.

Cancedda R, Giannoni P, Mastrogiacomo M. A tissue engineering approach to bone repair in large animal models and in clinical practice. Biomaterials 2007; 28: 4240-4250.

Chen G, Deng C, Li YP. TGF-beta and BMP signaling in osteoblast differentiation and bone formation. Int J Biol Sci 2012; 8: 272-288.

Cook SD, Baffes GC, Wolfe MW, Sampath TK, Rueger DC. Recombinant human bone morphogenetic protein-7 induces healing in a canine

long-bone segmental defect model. Clin Orthop Relat Res 1994: 302-312.

Dimitriou R, Jones E, McGonagle D, Giannoudis PV. Bone regeneration: current concepts and future directions. BMC Med 2011; 9: 66.

Fujihara K, Kotaki M, Ramakrishna S. Guided bone regeneration membrane made of polycaprolactone/calcium carbonate composite nano-fibers. Biomaterials 2005; 26: 4139-4147.

Gregory CA, Gunn WG, Peister A, Prockop DJ. An Alizarin red-based assay of mineralization by adherent cells in culture: comparison with cetylpyridinium chloride extraction. Anal Biochem 2004; 329: 77-84.

Guan J, Zhang J, Li H, Zhu Z, Guo S, Niu X, Wang Y, Zhang C. Human Urine Derived Stem Cells in Combination with beta-TCP Can Be Applied for Bone Regeneration. PLoS One 2015; 10: e0125253.

Hsu WK, Sugiyama O, Park SH, Conduah A, Feeley BT, Liu NQ, Krenek L, Virk MS, An DS, Chen IS, Lieberman JR. Lentiviral-mediated BMP-2 gene transfer enhances healing of segmental femoral defects in rats. Bone 2007; 40: 931-938.

Kang BJ, Ryu HH, Park SS, Koyama Y, Kikuchi M, Woo HM, Kim WH, Kweon OK. Comparing the osteogenic potential of canine mesenchymal stem cells derived from adipose tissues, bone marrow, umbilical cord blood, and Wharton's jelly for treating bone defects. J Vet Sci 2012; 13: 299-310.

Katz JM, Nataraj C, Jaw R, Deigl E, Bursac P. Demineralized bone matrix as an osteoinductive biomaterial and in vitro predictors of its biological potential. J Biomed Mater Res B Appl Biomater 2009; 89: 127-134.

Kondo N, Ogose A, Tokunaga K, Ito T, Arai K, Kudo N, Inoue H, Irie H, Endo N. Bone formation and resorption of highly purified beta-tricalcium phosphate in the rat femoral condyle. Biomaterials 2005; 26: 5600-5608.

Livak KJ, Schmittgen TD. Analysis of relative gene expression data using real-time quantitative PCR and the 2(-Delta Delta C(T)) Method. Methods 2001; 25: 402-408.

Long T, Zhu Z, Awad HA, Schwarz EM, Hilton MJ, Dong Y. The effect of mesenchymal stem cell sheets on structural allograft healing of critical sized femoral defects in mice. Biomaterials 2014; 35: 2752-2759.

Marino G, Rosso F, Cafiero G, Tortora C, Moraci M, Barbarisi M, Barbarisi A. Beta-tricalcium phosphate 3D scaffold promote alone osteogenic differentiation of human adipose stem cells: in vitro study. J Mater Sci Mater Med 2010; 21: 353-363.

Mauney JR, Jaquiery C, Volloch V, Heberer M, Martin I, Kaplan DL. In vitro and in vivo evaluation of differentially demineralized cancellous bone scaffolds combined with human bone marrow stromal cells for tissue engineering. Biomaterials 2005; 26: 3173-185.

Muller P, Bulnheim U, Diener A, Lüthen F, Teller M, Klinkenberg ED, Neumann HG, Nebe B, Liebold A, Steinhoff G, Rychly J. Calcium

phosphate surfaces promote osteogenic differentiation of mesenchymal stem cells. J Cell Mol Med 2008; 12: 281-291.

Nakamura A, Akahane M, Shigematsu H, Tadokoro M, Morita Y, Ohgushi H, Dohi Y, Imamura T, Tanaka Y. Cell sheet transplantation of cultured mesenchymal stem cells enhances bone formation in a rat nonunion model. Bone 2010; 46: 418-24.

Neupane M, Chang CC, Kiupel M, Yuzbasiyan-Gurkan V. Isolation and characterization of canine adipose-derived mesenchymal stem cells. Tissue Eng Part A 2008; 14: 1007-1015.

Pensak M, Hong S, Dukas A, Tinsley B, Drissi H, Tang A, Cote M, Sugiyama O, Lichtler A, Rowe D, Lieberman JR. The role of transduced bone marrow cells overexpressing BMP-2 in healing critical-sized defects in a mouse femur. Gene Ther 2015; 22: 467-475.

Reya T, Clevers H. Wnt signalling in stem cells and cancer. Nature 2005; 434: 843-850.

Ryu HH, Lim JH, Byeon YE, Park JR, Seo MS, Lee YW, Kim WH, Kang KS, Kweon OK. Functional recovery and neural differentiation after transplantation of allogenic adipose-derived stem cells in a canine model of acute spinal cord injury. J Vet Sci 2009; 10: 273-284.

Simpson RL, Wiria FE, Amis AA, Chua CK, Leong KF, Hansen UN, Chandrasekaran M, Lee MW. Development of a 95/5 poly(L-lactide-co-glycolide)/hydroxylapatite and beta-tricalcium phosphate scaffold as bone replacement material via selective laser sintering. J Biomed

Mater Res B Appl Biomater 2008; 84: 17-25.

Sugiyama O, An DS, Kung SP, Feeley BT, Gamradt S, Liu NQ, Chen IS, Lieberman JR. Lentivirus-mediated gene transfer induces long-term transgene expression of BMP-2 in vitro and new bone formation in vivo. Mol Ther 2005; 11: 390-398.

Vanhatupa S, Ojansivu M, Autio R, Juntunen M, Miettinen S. Bone Morphogenetic Protein-2 Induces Donor-Dependent Osteogenic and Adipogenic Differentiation in Human Adipose Stem Cells. Stem Cells Transl Med 2015; 4: 1391-1402.

Wang EA, Rosen V, D'Alessandro JS, Bauduy M, Cordes P, Harada T, Israel DI, Hewick RM, Kerns KM, LaPan P, Luxenberg DP, McQuaid D, Mountsatsos IK, Nove J, Wozney JM. Recombinant human bone morphogenetic protein induces bone formation. Proc Natl Acad Sci USA 1990; 87: 2220-2224.

Wei G, Ma PX. Structure and properties of nano-hydroxyapatite/polymer composite scaffolds for bone tissue engineering. Biomaterials 2004; 25: 4749-4757.

Wildemann B, Kadow-Romacker A, Pruss A, Haas NP, Schmidmaier G. Quantification of growth factors in allogenic bone grafts extracted with three different methods. Cell Tissue Bank 2007; 8: 107-14.

Xie Q, Wang Z, Huang Y, Bi X, Zhou H, Lin M, Yu Z, Wang Y, Ni N, Sun J, Wu S, You Z, Guo C, Sun H, Wang Y, Gu P, Fan X. Characterization of human ethmoid sinus mucosa derived mesenchymal stem cells

(hESMSCs) and the application of hESMSCs cell sheets in bone regeneration. Biomaterials 2015; 66: 67-82.

Yamato M, Okano T. Cell sheet engineering. Materials Today 2004; 7: 42-47.

Yu J, Tu YK, Tang YB, Cheng NC. Stemness and transdifferentiation of adipose-derived stem cells using L-ascorbic acid 2-phosphate-induced cell sheet formation. Biomaterials 2014; 35: 3516-3526.

Yun HS, Kim SH, Khang D, Choi J, Kim HH, Kang M. Biomimetic component coating on 3D scaffolds using high bioactivity of mesoporous bioactive ceramics. Int J Nanomedicine 2011; 6: 2521-2531.

국문초록

개의 결손골 모델에서 BMP-7 과발현 유도 중간엽 줄기세포 시트의 골재생 효과

김 용 선

(지도교수 권 오 경)

서울대학교 대학원

수의학과 수의외과학 전공

조직재생의학분야에서 성공적으로 골 결손을 치료하는 것은 매우 중요한 주제이다. 골재생을 위해서는 골분화 유도 세포, 골생성 관련 성장인자, 골생성 유도 기질 등이 필요하다. 중간엽 줄기세포와 중간엽 줄기세포 시트는 골 재생 능력이 우수하여, 골 결손을 치료하기 위한 하나의 방법으로 사용되고 있다. 골형성 단백질-7 (BMP-7)은 골 생성을 유도하는 역할을 한다. 또한 폴리 ε-카프로락톤(PCL)/β-인산삼석회(β-TCP)와 같은 폴리머/세라믹 지지체도 광범위한 골 결손을 치료하기 위해 사용된다.

첫 번째 실험에서는 개의 중간엽 줄기세포와 중간엽 줄기세포 시

트의 *in vitro* 골분화 능력을 비교하였다. 또한 PCL/β-TCP 지지체에 중간엽 줄기 세포를 이식하거나 골분화 유도 줄기세포 시트를 감싼 후에 개의 임계 크기 결손부에 이식하여 *in vivo* 골 재생의 확인 및 그 효과를 비교하였다. 미분화 줄기세포에 비해 골분화 유도 줄기세포와 골분화 유도 줄기세포 시트에서 알칼리성 인산가수 분해효소 활성도가 높게 측정되었고, 정량적 중합효소 연쇄반응 결과 골분화 관련 인자들이 높게 발현되는 것을 확인하였다. PCL/β-TCP 지지체와 골분화 유도 줄기세포 시트를 적용한 군에서 다른 군들에 비해 더 많은 신생골 형성을 확인하였다. 비록 골분화 유도 줄기세포와 골분화 유도 줄기세포 시트 사이에 *in vitro* 골분화 능력의 차이는 없었지만, *in vivo* 결과에서 지지체와 골분화 유도 줄기세포 시트를 적용한 군에서 미분화 줄기세포 또는 골분화 유도 줄기세포를 적용한 군들에 비해 더 많은 신생골이 형성되었다. 따라서 골분화 유도 줄기세포 시트는 개의 임계 크기 결손부의 치유를 돕는 골재생 유도 물질로 사용할 수 있다.

하지만 골분화 유도 줄기세포 시트는 2주 이상 배양하기 힘들고, 제작하기 어려운 반면, 미분화 줄기세포 시트는 배양하기 용이하였다. 따라서 다음 실험에서는 골분화 유도 줄기세포 시트 대신에 미분화 줄기세포 시트를 사용하였고, 골 분화 능력을 향상시키기 위하여 개의 BMP-7 유전자를 삽입한 줄기세포를 사용하여 미분화 줄

기세포 시트를 제작하였다. 또한 큰 결손부를 채우고, 골전도 효과를 높이기 위해서 탈회골기질을 함께 적용하였다.

두 번째 실험에서는 개의 중간엽 줄기세포에 BMP-7 유전자를 삽입하여, BMP-7 과발현 유도 줄기세포 시트를 제작하였다. 중간엽 줄기세포 시트와 BMP-7 과발현 유도 줄기세포 시트의 골분화 능력을 비교하고, PCL/β-TCP 복합체에 BMP-7 과발현 유도 줄기세포 시트를 감싼 후에 임계 크기 결손부에 이식하여 골 재생의 확인 및 비교하였다. 추가로 탈회골기질을 결손부 사이에 채워주었다. 중간엽 줄기세포 시트에 비해 BMP-7 과발현 유도 줄기세포 시트에서 알칼리성 인산가수 분해효소 활성도가 높게 측정되었고, 정량적 중합효소 연쇄반응 결과 골분화 관련 인자들이 높게 발현되는 것을 확인하였다. 또한 생체 내 골 결손 부위에 이식하였을 때, PCL/β-TCP 지지체와 BMP-7 과발현 유도 줄기세포 시트, 탈회골기질를 함께 적용한 군에서 더 많은 신생골 또는 신생 혈관을 형성하는 것을 확인하였고, 골 결손부에서 중간중간 석회화된 물질들이 확인되었다. 따라서 BMP-7 과발현 유도 줄기세포 시트와 탈회골기질 복합체는 개의 임계 크기 결손부의 치유를 돕는 골재생 유도 물질로 사용할 수 있다.

BMP-7 과발현 유도 중간엽 줄기세포 시트는 안정적으로 BMP-7을 생산하였고, 골분화 유도 인자와 혈관분화 유도 인자를 분비하

였다. 또한 골유도와 골전도 역할을 하는 탈회골기질과 함께 적용하여 효과적인 골재생 역할을 한 것으로 생각된다.

결론적으로 BMP-7 과발현 유도 중간엽 줄기세포 시트와 탈회골기질 복합체는 골 결손을 치료하는데 사용할 수 있으며, 조직재생분야에서 하나의 대체 치료법으로 사용하기에 적절하다고 사료된다.

주요어: 중간엽 줄기세포 시트, 골형성단백질-7, 탈회골기질, 골재생, 골 결손, 개

학번: 2009-21616